Monthly Notices of the ROYAL ASTRONOMICAL SOCIETY

MNRAS **532,** 1330–1344 (2024) https://doi.org/10.1093/mnras/stae1546
Advance Access publication 2024 June 29

Neutron star accretion events in AGN discs: mutimessenger implications

Shu-Rui Zhang,[1,2,3] Ye-Fei Yuan ,[1,2★] Jian-Min Wang[4] and Luis C. Ho[5,6]

[1]*School of Astronomy and Space Science, University of Science and Technology of China, Hefei 230026, China*
[2]*CAS Key Laboratory for Research in Galaxies and Cosmology, Department of Astronomy, University of Science and Technology of China, Hefei 230026, China*
[3]*Department of Physics and Earth Science, University of Ferrara, Via Saragat 1, I-44122 Ferrara, Italy*
[4]*Key Laboratory for Particle Astrophysics, Institute of High Energy Physics, Chinese Academy of Sciences, 19B Yuquan Road, Beijing 100049, China*
[5]*Kavli Institute for Astronomy and Astrophysics, Peking University, Beijing 100871, China*
[6]*Department of Astronomy, School of Physics, Peking University, Beijing 100871, China*

Accepted 2024 June 18. Received 2024 June 18; in original form 2024 March 27

ABSTRACT

This paper investigates the accretion of neutron stars (NSs) in active galactic nucleus (AGN) accretion discs. We classify potential accretion modes of NSs in AGN discs, proposing a hierarchical model of NS accretion: accretion flow from the Bondi sphere to accretion columns. The accretion of NSs in AGN discs differs from that of BHs, especially within the scale of the NS's magnetosphere due to its hard surface and magnetic field. As the accretion flow approaches the magnetosphere, the magnetic fields guide the accretion flow to form accretion columns, primarily dominated by neutrinos. While neutrinos generated from single NS accretion may not have observable effects, considering the all-sky background, they contribute to the neutrino background in the sub-MeV energy range comparable to that of supernova explosions. NS accretion may also lead to the generation of mass quadrupole moments, consequently generating gravitational waves (GWs). The GWs, which exhibit characteristic effects like periodic modulations and echoes, could be observed by third-generation GW detectors. The emission of neutrinos and GWs carries away energy and angular momentum brought by accretion, reducing the feedback effect on the AGN disc. This results in an exceptionally high NS accretion rate, leading to a collapse time-scale shorter than the migration-merge time-scale, making it less likely that binary NS mergers originate from AGN discs.

Key words: accretion, accretion discs – gravitational waves – neutrinos – quasars: supermassive black holes.

1 INTRODUCTION

Compact objects, including neutron stars (NSs), are believed to exist in the accretion discs of active galactic nuclei (AGNs) (Cheng & Wang 1999; Zhu et al. 2021), with a predicted high rate of NS–NS (black hloe (BH), white dwarf (WD)) mergers (McKernan, Ford & O'Shaughnessy 2020). While, in the high-density gas environment of AGN accretion discs, NSs are also prone to accrete and exceed their critical mass, leading to collapse (Perna et al. 2021). Nevertheless, the accretion mechanism of NSs in AGN discs has not been well studied. As a result, there is significant uncertainty about the lifetime of NSs in AGN discs, as well as the merger rate of binaries involving NSs. Observationally, the origins of gravitational wave (GW) sources involving NSs (Abbott et al. 2017, 2021) and low-mass gap compact objects (Özel et al. 2012; Abbott et al. 2020a, b) are uncertain. What are the observational effects of hyper-Eddington accretion in NSs and how crucial are their production of neutrinos (Zel'dovich, Ivanova & Nadezhin 1972; Ruffini & Wilson 1973) in neutrino astronomy? These profound questions, which encompass multiple messengers in extreme environments, are all intertwined with the accretion of NSs in AGN discs.

Bound stars around supermassive black hole (SMBHs) can originate from nuclear star clusters (Syer, Clarke & Rees 1991; Tagawa, Haiman & Kocsis 2020). These bound stars (or compact objects formed through evolution) interact continuously with the AGN disc, facilitating the exchange of angular momentum and energy between the compact objects and the disc (Ostriker 1983). Consequently, the orbits of compact objects are confined to the disc (Tanaka, Takeuchi & Ward 2002; Bartos et al. 2017; Yang et al. 2019; Fabj et al. 2020). Furthermore, stars can form in the outer region of the AGN disc ($\gtrsim 10^4 R_{\rm g}$, where $R_{\rm g}$ is defined as $GM_{\rm SMBH}/c^2$, and G is the gravitational constant, c is the speed of light) due to gravitational instability and subsequently evolve into compact objects (Stone, Metzger & Haiman 2017; Dittmann & Miller 2020; Derdzinski & Mayer 2023). Based on the distribution of progenitor star masses in AGN discs, a significant proportion is expected to evolve into NSs (Cantiello, Jermyn & Lin 2021; Dittmann, Cantiello & Jermyn 2021). Furthermore, massive stars evolving in AGN discs may have a higher fraction of magnetars, since high magnetic fields can be generated via dynamo processes, if the rotation rates are sufficiently high (Raynaud et al. 2020). And Jermyn et al. (2021) has shown that massive stars in AGN discs indeed evolve rotating very rapidly. Typically, the magnetic field may experience a decay process, such as Ohmic dissipation, during the accretion of NSs (Konar & Bhattacharya 1997; Pan & Yang 2021b). However, it is widely observed that AGN

★ E-mail: yfyuan@ustc.edu.cn

discs harbour coherent magnetic fields (Silant'ev et al. 2009; Daly 2019). When NSs accrete matter from AGN discs, due to magnetic flux conservation, the magnetic field of the NS may potentially be amplified during the accretion process. For NSs, the surface magnetic fields may play a crucial role in both spinning up and accelerating the accretion (Pan & Yang 2021b).

In the environment of AGN discs, where compact objects are subject to the combined effects of the disc gas and the gravitation of central SMBHs, various physical processes occur (Tagawa et al. 2020). The orbits of compact objects undergo migration (Bellovary et al. 2016; Pan & Yang 2021a), close encounters (Li, Lai & Rodet 2022b), collisions (Luo et al. 2023; Zhang et al. 2023), and scattering events (Samsing et al. 2022) occur among them. More particularly noteworthy phenomenon is accretion. Generally, the accretion pattern of compact objects in AGN discs exhibits an outer spherical and inner disc-like structure (Wang et al. 2021). Namely, at scales of the Bondi radius, accretion is nearly spherically symmetric, but within 1–2 orders of magnitude closer to the compact objects, the material circularizes to form an accretion disc (circum-CO disc) due to the differential rotation of the AGN discs (Pan & Yang 2021b). The circum-CO disc is dominated by outflows, and the feedback from these outflows on the gas in the AGN disc leads to intermittent accretion of compact objects (Wang et al. 2021; Chen, Ren & Dai 2023). Therefore, the average accretion rate of compact objects in the AGN disc is determined by the instantaneous accretion rate and the duty cycle. Nevertheless, in the environment of AGN discs, both the instantaneous and average accretion rates of compact objects far exceed the Eddington accretion rate.

The accretion of NSs in AGN discs differs from that of BHs, especially within the scale of the NS's magnetosphere due to its hard surface and magnetic field (Shapiro & Teukolsky 2008). The small radius and hard surface of a NS result in a mass-energy conversion efficiency during accretion that is about three times higher than that of a non-rotating BH. Under relatively high accretion rates, neutrinos may be emitted due to the production of positron–electron pairs (Zel'dovich et al. 1972; Ruffini & Wilson 1973; Houck & Chevalier 1991; Chevalier 1995). The strong magnetic field truncates the inner radius of the circum-NS disc, leading to a reduction in outflow feedback compared to BHs and an increase in net inflow rate (Chen et al. 2023). Furthermore, the magnetic field guides accreted material towards the polar cap region of the NS (Shapiro & Teukolsky 2008). This leads to a high accretion rate concentrated in relatively small areas. As a result, the polar cap is more prone to becoming extremely hot, which leads to a lower critical accretion rate for neutrino production (Mushtukov et al. 2018; Mushtukov, Ognev & Nagirner 2019). Neutrinos carry away a significant amount of energy, imposing an upper limit on electromagnetic radiation ($\sim$ Eddington luminosity) (Basko & Sunyaev 1976; Mushtukov et al. 2018). Therefore, this part of electromagnetic radiation feedback on the AGN disc (compared to outflow feedback from the circum-NS disc) can be neglected, as excess energy is carried away by neutrinos.

Moreover, under high accretion rates, NSs may drive the growth of a mass quadrupolar deformation, releasing GWs. Plausible mechanisms that may be at work include the creation of a 'mountain' (i.e. any kind of non-axisymmetric deformation that gives rise to a mass quadrupole) supported by the elastic crust (Bildsten 1998; Ushomirsky, Cutler & Bildsten 2000) or by magnetically supported mountains (Melatos & Payne 2005; Haskell et al. 2015) and unstable modes of oscillation of the star (Andersson 1998; Andersson, Kokkotas & Stergioulas 1999). However, current studies of NS accretion in AGN discs have not taken into account the production of neutrinos or GWs. This directly impacts the accretion rate and electromagnetic feedback, as they play crucial roles in the energy and angular momentum transfer during NS accretion. Additionally, this may lead to distinctive multimessenger observational effects, providing potential methods to verify the existence of compact objects in AGN discs.

The accretion rate of NSs in AGN discs further dictates the lifespan of NSs, thereby influencing the binary NS merger rate. The location in GW events of binary NS mergers, as well as the composition and formation mechanism of low-mass gap compact objects, remain to be determined. There is speculation that they may originate from AGN discs (Yang et al. 2020; Perna et al. 2021; Tagawa et al. 2021; Pan, Lyu & Yang 2022). Zhu et al. (2021) and Kathirgamaraju et al. (2023) examined the phenomenon of binary NS mergers in AGN discs. Perna et al. (2021) also calculated that the NS merger rate in AGN discs could reach $\sim 0.1 - 5\,\mathrm{Gpc^{-3}yr^{-1}}$, assuming the accretion rate of NSs is at the Eddington rate. However, these studies did not rigorously consider the impact of NS accretion. Additionally, if NSs can form binaries in AGN discs and their merger rates are significant (e.g. BH mergers in AGN discs may constitute up to ~ 80 per cent of the total merger rate of BHs; Ford & McKernan 2022), then a substantial total merger rate of NSs should be expected. However, as of now, ground-based GW observatories have detected nearly 200 GW sources (see the Gravitational-Wave Candidate Event Database; LIGO 2024), yet fewer than 1/10 of them are likely binary NS or NS-BH merger events, with the rest being binary BH merger events. Therefore, it is necessary to take into account the correct accretion rate in order to determine whether NSs in AGN discs are primarily driven by accretion-induced collapse or mergers.

This study aims to explore how NSs accreting in AGN discs, taking into account the impact of neutrinos and GWs production. It seeks to determine the accretion rate, and discuss potential observable multimessenger signals. The structure of this paper is as follows: In Section 2, the model of NS accretion in AGN discs is provided. Accretion behaviour at three different scales is discussed, with emphasis on the necessity and significance of multimessenger emission in NS accretion. Building on this model, Section 3 delves into the neutrino production during NS accretion and its potentially observational effects. Section 4 addresses the impact of NS accretion on GW signals, specifically encompassing GWs generated by NS rotation and those from binary NS mergers. Section 5 discusses the limitations of this study and provides prospects for further research. Finally, Section 6 concludes the paper.

Unless specified otherwise, tilde variables denote quantities of AGN discs distinct from variables associated with the NS and circum-NS disc. The convention of $Q_{\rm x} = Q/10^{\rm x}$ in cgs units are used. The standard ΛCDM cosmology, with $\Omega_{\rm m} = 0.315$, $\Omega_\Lambda = 0.685$, and $H_0 = 67.4\,\mathrm{km\ s^{-1}Mpc^{-1}}$ (Planck Collaboration VI 2020), is adopted.

2 ACCRETION MODELS AT DIFFERENT SCALES

In this section, we aim to demonstrate a hierarchical pattern in the accretion behaviour of NSs in AGN discs, as illustrated in Fig. 1. The following subsections will address models at various scales.

2.1 Bondi scale

The standard disc model (Shakura & Sunyaev 1973) summarized in Kato et al. (2008) is chosen to describe the AGN disc, this model is

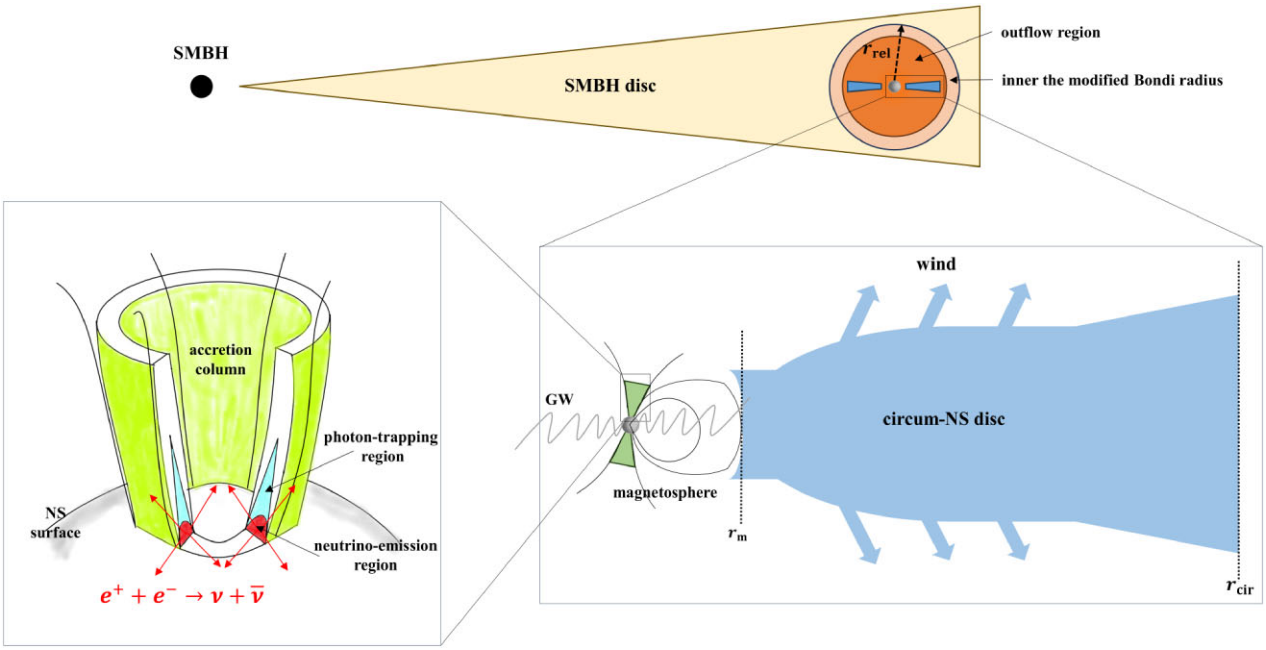

Figure 1. Schematic illustration of NS accretion in an AGN disc. Upper diagram: Accretion schematic at the Bondi Scale. Light orange indicates the inner region of the modified Bondi radius, while the dark orange represents the outflow region, which initially borders the circularization radius. The formation of the circum-NS disc within the circularization radius is depicted in blue. Lower right diagram: Zoomed-in illustration of the circum-NS disc and inside. The circum-NS disc is dominated by wind, with its outer radius denoted as the circularization radius ($r_{\rm cir}$) and inner radius as the magnetosphere radius ($r_{\rm m}$). The magnetic field guides accreted material to form accretion columns in the polar cap regions of the NS, depicted in green. The accreting NS may emit GWs, represented by the grey wave lines. Lower left diagram: Zoomed-in illustration of the accretion column. Blue denotes the photon-trapping region, while red represents the neutrino-emission dominated region. As the accretion rate increases, both the photon-trapping region and the neutrino-emission region will expand upwards, potentially disrupting the base of the hollow accretion column, which may then partially fill the centre-walled area and eventually form a solid column. Note that this diagram only shows the hollow accretion column, whereas the solid column with a cylindrical shape is not shown here.

akin to the one described in Sirko & Goodman (2003). This model includes both radiation and gas pressure, both Thompson and free–free opacity, and the effect of viscosity proportional to total pressure. But it does not include disc self-gravity. We expect this disc model to be a closer description of the inner parts ($\lesssim 10^4 R_{\rm g}$) of AGN discs in nature, while it may be inaccurate in the outer regions due to disc self-gravity, which leads to more complicated accretion processes and lacks a generally agreed-upon model. Therefore, our numerical calculations for AGN discs are within $2 \times 10^4 R_{\rm g}$. The fiducial parameters chosen in our computations include an accretion rate of $\dot{M} = 0.1\dot{M}_{\rm Edd}$ and a viscosity of $\tilde{\alpha} = 0.1$, where $\dot{M}_{\rm Edd}$ represents the Eddington rate. Because different SMBH masses and viscosity are the primary factors influencing the properties of AGN discs, and consequently, the accretion physics of NSs in it, AGN discs with varying SMBH masses and viscosity coefficients are also considered. For simplicity, a uniform density profile with a middle plane density $\tilde{\rho}_0$ is approximately adopted for vertical height $\tilde{Z}$ less than the disc scale height $\tilde{H}$ since the density decreases rapidly at $\tilde{Z} > \tilde{H}$ for a disc with an exponentially decaying density profile (Netzer 2013). The correction of star accretion in AGN discs with vertical structure can be referred to in Mac Low & McCray (1988), Dittmann et al. (2021), and Tagawa et al. (2022). The fiducial NS with a mass of 1.4 $M_\odot$ and a radius of 13 km is chosen. For different masses of NS, the volume–mass relation of a degenerate star, $m_{\rm ns} r_{\rm ns}^3 = {\rm const.}$, is maintained, where $m_{\rm ns}$ is the mass and $r_{\rm ns}$ is the radius of the NS. In this study, the Eddington accretion rate, denoted as

$$\dot{m}_{\rm Edd} = \frac{4\pi G m_{\rm ns} m_{\rm p}}{0.1\sigma_{\rm T} c} \approx 9.8 \times 10^{17} \left(\frac{m_{\rm ns}}{1.4{\rm M}_\odot}\right) {\rm g\ s^{-1}}, \quad (1)$$

is extensively used as the unit for accretion rates, where $m_{\rm p}$ is the proton mass and $\sigma_{\rm T}$ is the Thomson cross-section.

Given the AGN disc model, which specifies the physical properties of the AGN disc, with a NS embedded at a distance $\tilde{R}$ from the SMBH, we first examine the accretion behaviour of the NS on larger scales, namely the Bondi scale. Typically, accretion onto a star in uniform density gas is described by Bondi–Hoyle–Lyttleton (BHL) accretion (e.g. Shapiro & Teukolsky 2008). The BHL accretion radius is given by:

$$r_{\rm BHL} = \frac{G m_{\rm ns}}{\left(v_{\rm rel}^2 + \tilde{c}_{\rm s}^2\right)}; \quad (2)$$

And the BHL accretion rate is:

$$\dot{m}_{\rm BHL} = \frac{4\pi G^2 m_{\rm ns}^2 \tilde{\rho}_0}{\left(v_{\rm rel}^2 + \tilde{c}_{\rm s}^2\right)^{3/2}}. \quad (3)$$

Here, $v_{\rm rel}$ is the relative velocity between the NS and the surrounding gas, and $\tilde{c}_{\rm s}$ is the local sound speed of the AGN gas. The relative velocity is estimated as:

$$v_{\rm rel} = \frac{1}{2}\tilde{\Omega}_{\rm K} r_{\rm rel}, \quad (4)$$

where $\tilde{\Omega}_{\rm K}$ is the Keplerian angular velocity of the AGN disc, and $r_{\rm rel}$ is the modified Bondi radius. However, The accretion of the NS in AGN discs at the Bondi scale is not only determined by the BHL accretion rate, but also affected by the central SMBH tidal force and the thickness of the AGN disc. Therefore, the modified Bondi radius, representing the radius of the accretion cylinder, is given by:

$$r_{\rm rel} = \min\{r_{\rm BHL}, r_{\rm Hill}\}, \quad (5)$$

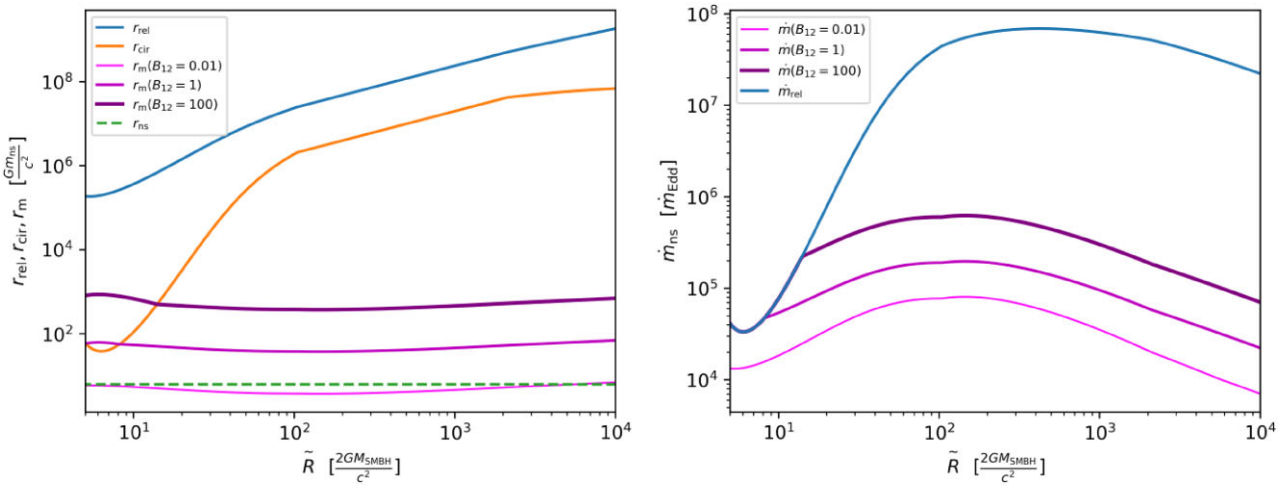

Figure 2. The left panel displays different radius scales varying with AGN disc radii $\tilde{R}$ in the fiducial model. The Bondi scale (equation 5), circularization radius, and magnetosphere radii are represented by blue, yellow, and purple curves, respectively. Additionally, the shades of purple, ranging from dark to light, correspond to magnetosphere radii with varying magnetic field strengths, from strong to weak. The right panel displays accretion rates at different scales varying with AGN disc radii the fiducial model. The blue curve represents the accretion rate at the Bondi scale (equation 6), while the purple curve denotes the accretion rate at the magnetosphere, with darker shades indicating stronger magnetic fields and lighter shades indicating weaker ones. In this study, the fiducial parameters consist of: $M_{\rm SMBH} = 10^8 {\rm M}_\odot$, $\tilde{\alpha} = 0.1$, $\dot{M} = 0.1\dot{M}_{\rm Edd}$, $m_{\rm ns} = 1.4{\rm M}_\odot$, $r_{\rm ns} = 13\,{\rm km}$, and $s = 0.5$ in equation (10).

where the Hill radius is defined as $r_{\rm Hill} = (m_{\rm ns}/3M_{\rm SMBH})^{1/3}\,\tilde{R}$. The corresponding modified Bondi accretion rate is denoted as (Pan & Yang 2021b):

$$\dot{m}_{\rm rel} = \min\{1, \frac{\tilde{H}}{r_{\rm Hill}}\} \times \min\{1, \frac{r_{\rm Hill}}{r_{\rm BHL}}\} \times \dot{m}_{\rm BHL}, \tag{6}$$

which represents the correct inflow rate at the Bondi scale.

The blue curves in Fig. 2 depict the modified Bondi radii and the corresponding modified Bondi accretion rates at different AGN radial positions in the fiducial model. Overall, the accretion rates of NSs at the Bondi scale are strikingly high, $\gtrsim 10^5\dot{m}_{\rm Edd}$ and spanning about three orders of magnitude. The accretion flow at this scale is approximately radially infalling, but as the accreted material moves inward, it gradually undergoes circularization due to differential rotation of the AGN disc.

2.2 Circum-NS disc

The accreted material gradually undergoes circularization, forming a circum-NS disc. The circularization radius, $r_{\rm cir}$, can be estimated based on angular momentum conservation using

$$(Gm_{\rm ns}r_{\rm cir})^{\frac{1}{2}} = v_{\rm rel}(r_{\rm rel})r_{\rm rel}. \tag{7}$$

The outer radius of the circum-NS disc corresponds to the circularization radius, with an accretion rate at the outer boundary equal to the modified Bondi accretion rate $\dot{m}_{\rm rel}$. This implies a reasonable assumption that there is no outflow loss between $r_{\rm rel}$ and the circularization radius $r_{\rm cir}$. The circularization radius in the fiducial model is depicted by the yellow curve in Fig. 2. Typically, it is smaller by 1–2 orders of magnitude compared to the modified Bondi radius. However, in the inner region of the AGN disc, the circularization radius undergoes a sharp reduction. This is because in the inner region of the AGN disc, the sound speed $\tilde{c}_{\rm s}$ increases sharply, resulting in a decrease in $r_{\rm rel}$, subsequently leading to a significant reduction in $r_{\rm cir}$, as supported by equations (2) and (7).

It's worth noting that although the accretion rate of the circum-NS disc is very high, it is still insufficient to trigger neutrino emission. The critical accretion rate for neutrino-dominated disc accretion can be estimated as (Chevalier 1996)

$$\dot{m}_{\rm cn} = \max\{\dot{m}_{\rm cn1}, \dot{m}_{\rm cn2}\}, \tag{8}$$

where

$$\dot{m}_{\rm cn1} = 23.0\,\beta_1^{-0.22}\left(\frac{\kappa}{0.2\,{\rm cm^2 g^{-1}}}\right)^{-0.73} \times \left(\frac{n_{\rm ns}}{1.4{\rm M}_\odot}\right)^{-0.03} \times \left(\frac{r_{\rm cir}}{10^{10}\,{\rm cm}}\right)^{1.08} {\rm M}_\odot{\rm yr}^{-1}, \tag{9a}$$

$$\dot{m}_{\rm cn2} = 8.2\times10^{11}\beta_1^{-0.80}\left(\frac{r_{\rm rel}}{10^{11}\,{\rm cm}}\right)^{-2.70} \times \left(\frac{n_{\rm ns}}{1.4{\rm M}_\odot}\right)^{-0.10} \times \left(\frac{r_{\rm cir}}{10^{10}\,{\rm cm}}\right)^{4.0} {\rm M}_\odot{\rm yr}^{-1}, \tag{9b}$$

with β_1 of the order of unity and a gas opacity $\kappa \approx 0.34\,{\rm cm^2 g^{-1}}$. In above equations, $\dot{m}_{\rm cn1}$ sets the condition for the shock radius of the disc equating the photon trapping radius, and $\dot{m}_{\rm cn2}$ sets the condition for the shock radius of the disc equating the modified Bondi radius $r_{\rm rel}$. Fig. 3 compares the estimated Bondi accretion rate with the critical accretion rate for neutrino-dominated disc accretion. It can be observed that the circum-NS disc is far from capable of generating neutrinos.

Actually, hyper-Eddington accretion in the circum-NS disc is dominated by outflows. The relationship between the inflow rate and the radius of the circum-NS disc is assumed to be (e.g. Blandford & Begelman 1999; Chen et al. 2023)

$$\dot{m}_{\rm in}(r) = \dot{m}_{\rm cir}\,(r/r_{\rm cir})^s\,, \tag{10}$$

where s is a free parameter lying in $0 < s \leqslant 1$, and $s = 0.5$ is the fiducial parameter in this work. As this scale is primarily feedback by outflows, it directly impacts the inflow rate and feedback strength to AGN disc, consequently influencing the merger rate of NSs in the AGN disc. Although the circum-NS disc cannot produce neutrinos, when the NS accretion approaches spherical symmetry, or when it undergoes column accretion under the influence of magnetic fields, it significantly reduces the critical accretion rate for neutrino production.

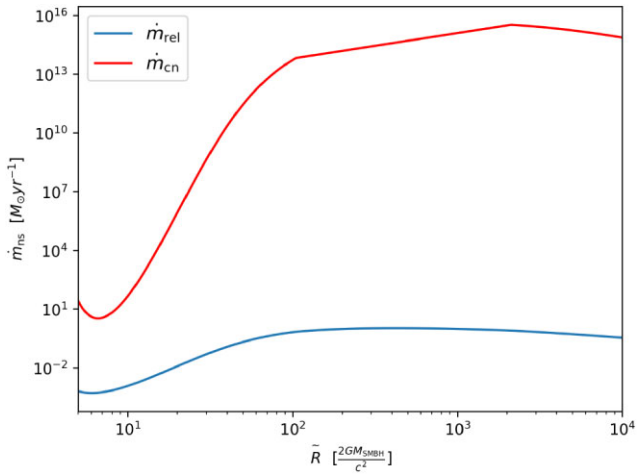

Figure 3. Comparison between the accretion rate at the outer boundary of the circum-NS disc and the critical accretion rate for neutrino-dominated discs. The accretion rate at the outer boundary of the circum-NS disc is the modified Bondi accretion rate, which is identical to the one in Fig. 2.

2.3 Inner the magnetosphere

The accretion of NSs in AGN discs exhibits unique characteristics within the magnetosphere of NS. There are two notable factors: the magnetic field and the solid surface of the NS. The magnetic field of the NS is commonly assumed to be dipolar. The inner radius of the circum-NS disc is determined by the strength of the magnetic field. When the gas pressure within the circum-NS disc exceeds the magnetic pressure, the magnetic field truncates the circum-NS disc at the magnetosphere radius $r_{\rm m}$, the so-called Alfvén radius.[1] Hence, the inner radius of the circum-NS disc is determined by

$$\frac{B(r_{\rm m})^2}{8\pi} = \rho(r_{\rm m})v(r_{\rm m})^2. \tag{11}$$

As a qualitative estimate, assume steady, transonic flow at nearly free-fall velocity (Shapiro & Teukolsky 2008)

$$v(r) = \left(\frac{Gm_{\rm ns}}{r}\right)^{\frac{1}{2}}, \tag{12a}$$

$$\rho(r) = \frac{\dot{m}_{\rm in}(r)}{4\pi v r^2}. \tag{12b}$$

Substituting equation (10), the inner radius of the circum-NS disc can be estimated as

$$r_{\rm m} = \left(\frac{B_0^4 r_{\rm ns}^{12} r_{\rm cir}^{2s}}{Gm_{\rm ns}\dot{m}_{\rm rel}^2}\right)^{\frac{1}{7+2s}}, \tag{13}$$

where B_0 is the dipole magnetic field strength at NS surface. Therefore, the accretion rate reaching the surface of the NS is denoted as $\dot{m} = \dot{m}_{\rm in}(r_{\rm m})$, assuming no outflows from the inner radius of the circum-NS disc to the surface of the NS due to the magnetic field.

In Fig. 2, in addition to providing $r_{\rm rel}$ and $r_{\rm cir}$ (outer radius of the circum-NS disc) as well as $\dot{m}_{\rm rel}$ (accretion rate at the outer radius), it also gives the inner radius of the circum-NS disc and its corresponding accretion rate for different magnetic field strengths. Overall, the computed results support the hierarchical accretion pattern depicted in Fig. 1. Usually, inwards from the modified Bondi radius, matter is gradually circularized to form the circum-NS disc, and it is only further inwards that truncation of the inner radius occurs, i.e. $r_{\rm cir} > r_m$. However, in the inner region of the AGN disc, $r_{\rm cir} < r_m$, indicating that the accretion flow is truncated by the magnetic field before circularization. In this pattern, nearly spherically accretion prevails beyond the magnetosphere, and the component of the circum-NS disc depicted in Fig. 1 disappears. This nearly spherical accretion flow, guided by the magnetic field, forms a solid accretion column (i.e. flow filling the whole column) above the polar cap of the NS, whereas accretion with a circum-NS disc leads to a hollow accretion column (i.e. a thin sidewall) as shown in Fig. 1. Fig. 4 presents the various scale radii and accretion rates for different parameters relative to the fiducial model, qualitatively resembling the fiducial model. In summary, for the majority of cases, the hierarchical model in Fig. 1 is supported, and the accretion rate at the inner radius remains hyper-Eddington.

Due to its hard surface, NSs can achieve high mass-energy conversion efficiencies. As an example, for the fiducial NS ($m_{\rm ns} = 1.4M_\odot$ and $r_{\rm ns} = 13$km), it can reach an efficiency given by:

$$\eta = 1 - \left(1 - \frac{2Gm_{\rm ns}}{r_{\rm ns}c^2}\right)^{\frac{1}{2}} \approx 17.4 \ \text{per cent}, \tag{14}$$

assuming the space–time outside the NS surface is Schwarzschild space–time. This efficiency is slightly modified compared to the efficiency of approximately 15.9 per cent in Newtonian space–time. For comparison, the efficiency of nuclear fusion only reaches up to 0.7 per cent and for a Schwarzschild Black hole it is up to 5.7 per cent. If the accretion material is ionized hydrogen, and all gravitational potential energy is converted into internal energy in the accretion column without loss, it has:

$$\eta m_{\rm p}c^2 = 2 \times \frac{3}{2}k_{\rm B}T, \tag{15}$$

where $k_{\rm B}$ is the Boltzmann constant. An extremely high temperature can result at the base of the column due to the exceedingly high mass accretion rate, with $T \approx 6.3 \times 10^{11}$K ≈ 54 MeV, consequently leading to energy losses due to neutrino emission. Because neutrinos take away some of the energy, the temperature does not get that high in reality. The primary mechanism for neutrino production is the annihilation of electron–positron pairs. Additionally, there are contributions from bremsstrahlung, plasmon decay, photoneutrinos, and synchrotron neutrino production (Bernal, Lee & Page 2010). However, their contributions are not significant when compared to the annihilation of pairs (Mushtukov et al. 2018); and the magnetic field has a minor correction to the neutrino production rate from the annihilation of pairs (Kaminker et al. 1992).

The neutrino luminosity can be calculated by counting the portion of photons trapped in the advection-dominated accretion column. This is approximated as (Asthana et al. 2023)

$$L_\nu \approx 0.64\,\eta\dot{m}c^2 \arctan\left(\frac{\eta\dot{m}c^2}{8\times 10^{40}\ \text{erg s}^{-1}}\right). \tag{16}$$

When L_ν exceeds half of $\eta\dot{m}c^2$, it is considered neutrino-dominated accretion. The critical accretion rate for neutrino-dominated columnar accretion is thus $\dot{m}_{\rm cn} \sim 500\dot{m}_{\rm Edd}$. Obviously, this condition is easily met for accretion onto NSs in AGN discs. Additionally, the non-axisymmetric accretion, as well as the asymmetry in nuclear reactions of the accreted material, results in the NS's crust possessing a mass quadrupole. Moreover, the magnetic field may contribute further to the asymmetry of the mass quadrupole, leading to the generation of GWs.

[1]Note that in some studies, the magnetospheric radius where the accretion flow is truncated is not exactly equal to the Alfvén radius where the gas pressure equals the magnetic pressure; the two may differ by a factor of the order of unity.

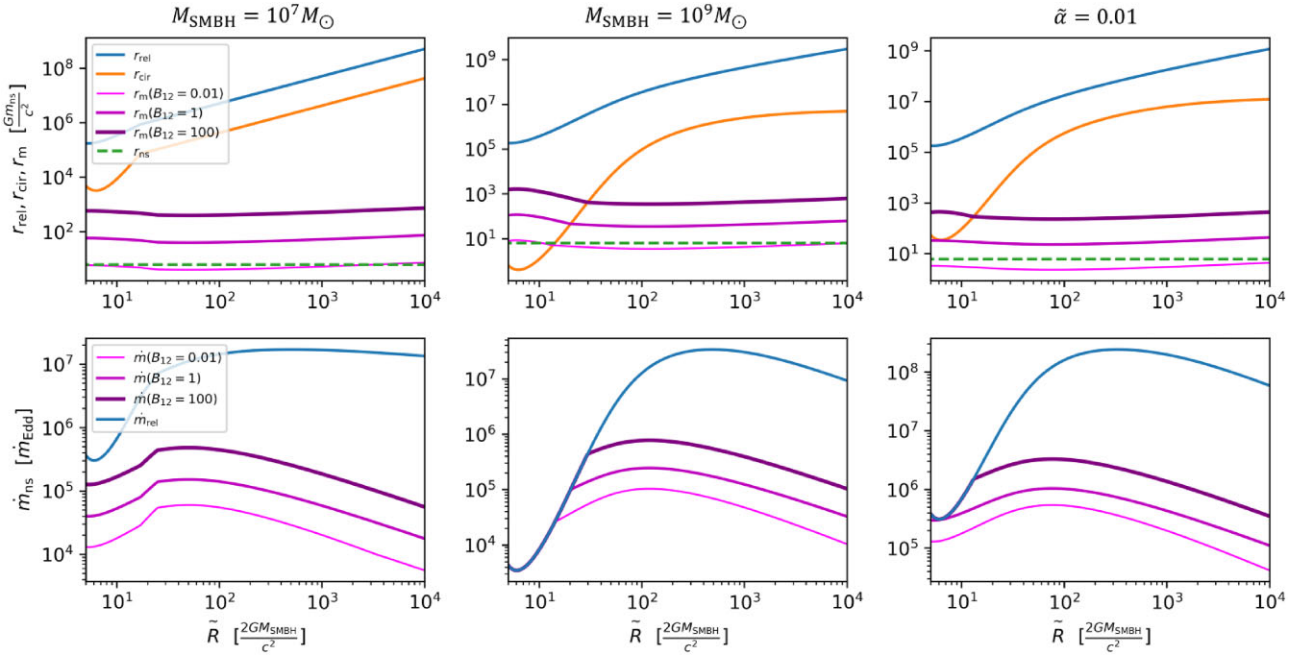

Figure 4. Accretion scales and rates of NSs in AGN discs for parameters different from the fiducial model are depicted. The top row displays various radius scales, while the bottom row illustrates accretion rates corresponding to these different scales. In the panels from left to right, the parameters are only altered as $M_{\rm SMBH} = 10^7 {\rm M}_\odot$, $M_{\rm SMBH} = 10^9 {\rm M}_\odot$, and $\tilde{\alpha} = 0.01$, respectively, while the remaining parameters remain consistent with the fiducial model. Each curve corresponds to the same description as in Fig. 2.

In short, high accretion rates, combined with efficient energy conversion and the formation of an accretion column, can trigger neutrino production, as well as potentially lead to the generation of GWs. Due to the substantial optical depth of AGNs, significant observable effects from electromagnetic radiation may be scarce (see more in Section 5 and the supplementary material). However, scales within the magnetosphere could produce multimessenger signals, potentially resulting in observable effects of the presence of NSs in AGN discs.

3 ON THE ROLES OF NEUTRINOS

3.1 Classification of accretion

We have studied the accretion of NSs in AGN discs with the hierarchical pattern shown in Fig. 1, which is generally consistent in AGN discs. However, the AGN disc environment covers a wide range of possible parameters, and different magnetic fields, angular momenta, and accretion rates may result in slight variations or reveal more detailed features in the NS accretion pattern. In this section, a more comprehensive classification of NS accretion in AGN discs is provided, with a particular focus on the production of neutrinos.

Fig. 5 classifies possible accretion scenarios and neutrino production based on angular momentum, magnetic field, and accretion rate. It is divided into two major categories. When the accreted matter has enough angular momentum to form a circum-NS disc, accretion exhibits three hierarchical modes. However, when the angular momentum of the accreted matter is insufficient, the circum-NS disc disappears, and the accretion remains nearly spherical until it reaches the magnetic layer or the NS surface. The red boxes in the last column of the Fig. 5 indicate cases of neutrino-dominated accretion, while the green boxes represent situations where neutrinos are not significantly generated. It is worth noting that in the case of

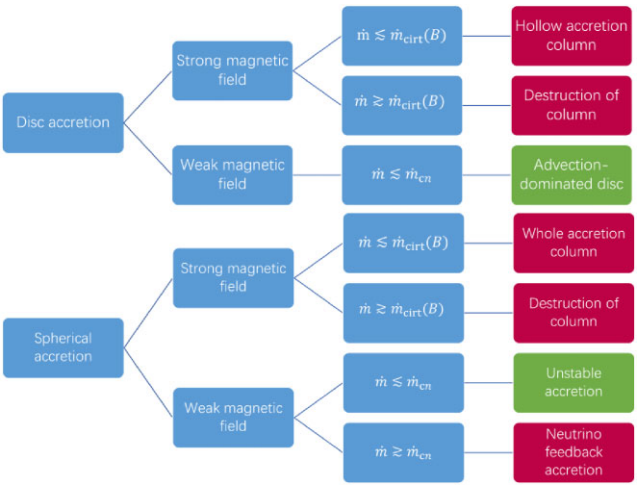

Figure 5. Classification of accretion patterns of NSs in AGN discs and their neutrino production based on the angular momentum of the accretion flow, magnetic field strength, and accretion rate. The red boxes in the right column signify neutrino-dominated accretion, while the green boxes indicate accretion with minimal neutrino production. The strong magnetic field specifically refers to a significantly larger Alfvén radius compared to the radius of the NS.

'Disc accretion–Weak magnetic field – $\dot{m} \lesssim \dot{m}_{\rm cn}$', a green box is used to indicate that significant neutrino emission is not expected. However, neutrino-cooled accretion may occur in a non-steady manner (Chevalier 1996). Furthermore, $\dot{m}_{\rm crit}(B, S)$ and $\dot{m}_{\rm cn}$ are not constant values. The critical accretion rate $\dot{m}_{\rm crit}(B, S)$ that disrupts the column bottom depends not only on the magnetic field but also on whether a circum-NS disc is present (i.e. different cross section S), as detailed in equation (19). On the other hand, the critical accretion

rate for neutrino-dominated accretion, denoted as $\dot{m}_{\rm cn}$, is determined by how the accretion flow reaches the NS surface. It is categorized into three groups: spherical accretion with $\dot{m}_{\rm cn} \gtrsim 10^4 \dot{m}_{\rm Edd}$ (Chevalier 1989); disc accretion, where $\dot{m}_{\rm cn}$ significantly exceeds the accretion rate in AGN discs; and accretion column with $\dot{m}_{\rm cn} \sim 500\dot{m}_{\rm Edd}$.

Considering the specific circumstances of AGN discs, in Fig. 5, we do not just simply list all possible cases of NS accretion found in the literature. For instance, the scenario of 'Disc accretion–Weak magnetic field – $\dot{m} \gtrsim \dot{m}_{\rm cn}$' has not been included because, as depicted in Fig. 3, this situation is not feasible in AGN discs; it is only likely to occur in cases of higher accretion rates during supernova fallback accretion (Chevalier 1996). Additionally, the case of $\dot{m} \lesssim \dot{m}_{\rm cn}$ under strong magnetic fields (column accretion $\lesssim 500\dot{m}_{\rm Edd}$, with no significant neutrino production) has not been listed because the likelihood of this occurring in AGN discs is very low, as shown in Figs 2 and 4. Nevertheless, this scenario could still manifest during intermittent accretion when a cavity formed.

Accretion patterns vary at different radii of AGN discs. In the inner regions of AGN discs, owing to the higher sound speed, accretion typically exhibits spherically symmetric characteristics, whereas in the outer regions of AGN discs, a circum-NS disc is generally formed. The accretion rate reaching the NS is relatively low in both the very inner and outer regions, usually peaking around $\sim 100R_{\rm g}$. In summary, with very few exceptions, accretion of NSs in AGN discs is dominated by neutrino emission.

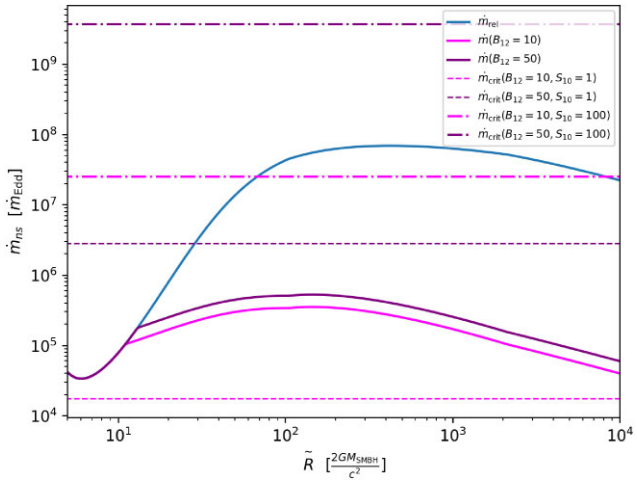

Figure 6. Comparison between the accretion rates of NSs in the AGN disc and the critical accretion rate for disrupting the bottom of columns. The blue line, identical to the right panel of Fig. 2, represents the accretion rate at the Bondi scale in the fiducial model. The solid purple lines depict the accretion rates reaching the inner radius of the circum-NS disc for different magnetic field strengths. The dashed lines indicate the critical accretion rate for disrupting the hollow column bottom, while the dash-dotted lines indicate it for the solid column bottom.

3.2 Column bottom destruction and neutrino energy spectrum

Let's delve into more details, starting with the column on accretion, regarding the general case. When the accretion rate exceeds the critical accretion rate of $\gtrsim 500\dot{m}_{\rm Edd}$, the electromagnetic luminosity produced by the accretion column reaches its peak value, which is $\gtrsim L_{\rm Edd}$ (Basko & Sunyaev 1976; Mushtukov et al. 2018). Although the peak luminosity is highly sensitive to the accretion geometry and can surpass the Eddington luminosity $L_{\rm Edd}$, it remains negligible compared to the gravitational potential energy released from accretion. This is because when the accretion rate far exceeds the Eddington limit, the accretion column becomes optically thick to the generated photons, causing the majority of them to be unable to escape laterally. Instead, they are advected along with the matter and trapped at the base of the column, resulting in a significantly higher radiation energy density and temperatures. At sufficiently high temperatures, energy losses due to neutrino emission become more effective than those through photons. In strong magnetic fields, neutrino emission carries away all the excess energy flux.

The scale height of the accretion column is characterized by the position of the shock in it. The shock rises upwards with increasing accretion rate until it either (i) reaches the Alfvén surface, or (ii) the ram pressure of the accreting flow approaches the magnetic pressure at the stellar surface (Basko & Sunyaev 1976). In other words, when the accretion rate increases, the bottom of accretion column may be disrupted. Given a number density of proton at column bottom $n_{\rm p}$, the critical temperature $T_{\rm crit}(B, S)$ for disruption can be solved from

$$P_{\rm tot}(S, B, T) < P_{\rm crit}(B, T), \tag{17}$$

where

$$P_{\rm crit} \approx 3 \times 10^{23} S_{10}^{1/2} B_{12}^2 T_{10}^{-1}\ {\rm erg\ cm^{-3}}, \tag{18a}$$

$$P_{\rm tot} = P_{\rm gas} + P_{\rm rad} = nk_{\rm B}T + \frac{1}{3}aT^4, \tag{18b}$$

are the critical pressure for column disrupted (Bildsten & Brown 1997) and the total pressure, respectively. Here, S is the cross-section of accretion column, n is the massive particle number density $n = n_{\rm p} + n_+ + n_-$, and a is the radiation constant. For a hollow accretion column, $S \sim 10^{10}{\rm cm}^2$, and for a solid accretion column, $S \sim 10^{12}{\rm cm}^2$. It is worth noting that $T_{\rm crit}$ is insensitive to $n_{\rm p}$, and $n_{\rm p} = 5.98 \times 10^{29}{\rm cm}^{-3}$ (i.e. $\rho = 10^6{\rm g\ cm}^{-3}$) is chosen for calculation. The number densities of electrons and positrons $n_{\mp}(T, B)$ in the equilibrium can be determined by integrating the longitudinal momentum distribution function and summing over all Landau levels (e.g. Kaminker et al. 1992; Harding & Lai 2006; Mushtukov et al. 2018). We calculate $n_{\mp}$ numerically under the assumption of completely ionized hydrogen plasma following Mushtukov et al. (2018). The height of the region where neutrinos are produced does not exceed the scale height of the accretion column, which is within the magnetosphere. Therefore, the upper limit of accretion rate $\dot{m}_{\rm crit}$ can be got from

$$r_{\rm m}(B, \dot{m}) S Q_\nu^-(T_{\rm crit}) \gtrsim \frac{\eta \dot{m} c^2}{2}, \tag{19}$$

where energy losing rate due to pairs annihilation can be estimated as

$$Q_\nu^- \sim 4 \times 10^{24} T_{10}^9\ {\rm erg\ cm^{-3}s^{-1}} \tag{20}$$

for the temperature range $T \gtrsim 10^9{\rm K}$ and magnetic field strength range $B \lesssim 10^{15}{\rm G}$ (Kaminker et al. 1994).

As shown in Fig. 6, in AGN discs, NS accretion can easily disrupt the bottom of a hollow accretion column if $B \lesssim 5 \times 10^{13}$ G. Once the bottom of the hollow column is disrupted, the material flow spreads beyond the constraints of the column wall, partially filling the hollow column and asymptotically forming a solid one. The destruction of the solid accretion column bottom in NS accretion in AGN discs is challenging due to its larger cross section (S) and higher critical pressure ($P_{\rm crit}$), as indicated by equations (18) and (19). For the same reason, in the case of absence of the circum-NS disc in the inner region of AGN disc, the initially formed solid column is insufficient to be disrupted.

Table 1. Critical temperature and accretion rate leading to the disruption of the bottoms of hollow columns ($S \sim 10^{10}\mathrm{cm}^2$) under varying dipole magnetic field strengths of a NS.

B(G)	10^{13}	5×10^{13}	10^{14}	2×10^{14}
$T_{\rm crit}$(K)	9.43×10^9	1.76×10^{10}	2.32×10^{10}	3.05×10^{10}
$\dot{m}_{\rm crit}(\dot{m}_{\rm Edd})$	1.82×10^4	2.93×10^6	2.76×10^7	2.55×10^8

Table 1 provides examples of the critical temperature and critical accretion rate for spreading over the NS surface at the bottom of hollow accretion columns corresponding to different magnetic field strengths. It can be observed that the critical accretion rate for these columns is sensitive to the magnetic field, while the critical temperature is less affected by it. The critical temperature at the bottom of the column is generally maintained at around 1 MeV, with a narrow distribution, as the neutrino emission rate is highly sensitive to temperature, as given by equation (20). Lower temperatures would require a significantly larger neutrino emission region beyond the cross section of the accretion column. On the other hand, assuming higher temperatures would disrupt the bottom of the column, leading to an increase in the column cross section. Consequently, there would be an expanded neutrino emission region. This prevents a significant rise in temperature, contradicting the assumption of increased accretion rate leading to a significant temperature rise. Therefore, the neutrino energy spectra is concentrated within a narrow energy range, with a characteristic temperature of ~ 1 MeV at the position of neutrino production.

Once the temperature is determined, the average energy and the spectrum of neutrinos produced can be calculated. Neutrinos produced from NS accretion are characterized by the annihilation of electron–positron pairs, and the environment is optically thin to neutrinos. In this case, the normalized spectrum is given by Misiaszek, Odrzywołek & Kutschera (2006), as

$$\phi(E_\nu; \langle E_\nu\rangle, \sigma_\nu^2) = \frac{\left(\langle E_\nu\rangle^2/\sigma_\nu^2\right)^{\langle E_\nu\rangle^2/\sigma_\nu^2}}{\Gamma\left(\langle E_\nu\rangle^2/\sigma_\nu^2\right)} \frac{E_\nu^{\langle E_\nu\rangle^2/\sigma_\nu^2-1}}{\langle E_\nu\rangle^{\langle E_\nu\rangle^2/\sigma_\nu^2}} \exp\left(-\frac{\langle E_\nu\rangle E_\nu}{\sigma_\nu^2}\right). \quad (21)$$

Here $\langle E_\nu\rangle(T)$ and $\sigma_\nu^2(T)$ are the average energy of neutrinos and the variance of neutrino energy respectively, and it can be found in the tables of PSNS (2001) and Misiaszek et al. (2006). However, neutrinos generated near the surface of the NS experience gravitational redshift, leading to the observed neutrino spectrum at an infinite distance, given by:

$$\phi_\infty(E_\nu) = (1+z_{\rm g})\phi\left((1+z_{\rm g})E_\nu\right), \quad (22)$$

where

$$1 + z_{\rm g} = \left(1 - \frac{2Gm_{\rm ns}}{r_{\rm ns}c^2}\right)^{-\frac{1}{2}} \quad (23)$$

is the gravitational redshift factor. Also, the average energy of neutrinos shifts to $\frac{\langle E_\nu\rangle}{1+z_{\rm g}}$. The key parameter of these spectra is the temperature. As discussed above, the temperature of the NS accretion in AGN discs remains at ~ 1 MeV.

In Fig. 7, spectra observed by a distant observer with temperatures of 0.5 MeV, 1 MeV, and 1.5 MeV are provided. The corresponding average energies of neutrinos near the NS surface are 2.26 MeV, 4.11 MeV, and 6.16 MeV, respectively. After gravitational redshift, the corresponding average energies are 1.88 MeV, 3.40 MeV, and 5.09 MeV, respectively. To first order, there are no differences between the spectra of different neutrino flavours (i.e. e, μ, τ-neutrino flavour) (Misiaszek et al. 2006). These obtained spectra can be used for the neutrino background calculations.

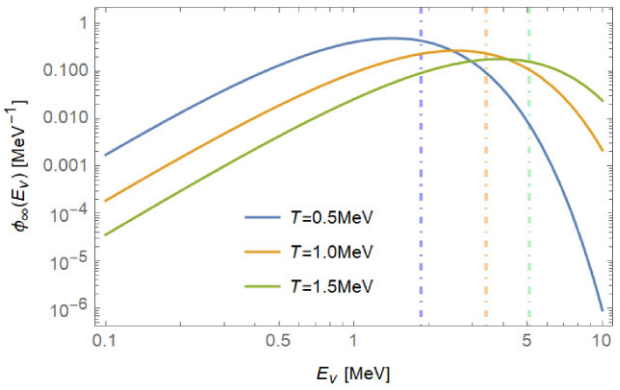

Figure 7. Normalized neutrino energy spectra (solid line) and average energy (dot-dashed line) produced by NS accretion observed by a distant observer. Different colours correspond to various temperatures of the hot plasma at the neutrino generation location.

3.3 Neutrino background at MeV scope

We first estimate the detectability of neutrinos produced by a single NS accretion in a nearby AGN disc using the Hyper-Kamiokande (HK) detector. The detection rate of neutrino events depends on the sensitivity of the detector, the distance to the neutrino source, the luminosity of the neutrino source, and the accumulated detection time. The number of events can be estimated as (Scholberg 2015):

$$N_{e\nu} \simeq \frac{t}{4\pi d^2\langle E_\nu\rangle} \frac{V_{\rm det} N_{\rm A}\rho_{\rm N}\sigma_{\rm cc}^{\bar{\nu}_e p} L_\nu}{6}, \quad (24)$$

where $N_{\rm A}$ is the Avogadro's number, $\rho_{\rm N} = 2/18\mathrm{g\ cm}^{-3}$ is the nucleons density in water (Mohapatra & Pal 2004), $\sigma_{\rm cc}^{\bar{\nu}_e p} \simeq 9 \times 10^{-44} E_\nu^2\ \mathrm{MeV}^{-2}$ is the cross-section (Bahcall 1989), and the division by six accounts for neutrino oscillations. We evaluate the HK with a water volume of $V_{\rm det} = 560$ Kton (Abe et al. 2011; Scholberg 2015) to detect a NS accretion in a nearby AGN with a distance of $d \sim 5$Mpc. The neutrino luminosity is estimated to be $L_\nu \sim 2 \times 10^5 L_{\rm Edd}$, and with a detection time of $t = 10$ yr, the expected number of events is only $N_{e\nu} \sim 10^{-3}$. It is obvious that existing detectors, as well as those in the near future, are incapable of detecting individual events of NS accretion in AGN discs. In fact, the energy released from the accretion of NSs in AGN discs is predominantly carried away by neutrinos. The estimated neutrino emission from a NS, from its birth to collapse, is approximately $\eta \mathrm{M}_\odot c^2 \sim 3 \times 10^{53}$erg, which is equivalent to the total neutrino energy generated by a core–collapse supernova. The reason why core–collapse supernovae are easily detectable is due to their rapid release of nearly all neutrinos within ~ 10s (Kotake, Sato & Takahashi 2006), whereas the neutrinos emitted from the accretion of NSs in AGN discs occur at a much slower rate.

While individual events may be challenging to detect, the neutrino background produced by NS accretion in AGN discs across the entire sky is worth exploring. Similar to the contribution of neutrinos from supernova to the background (Horiuchi, Beacom & Dwek 2009; Beacom 2010), the number flux of neutrinos from NS accretion in all-sky AGNs is estimated as

$$\frac{{\rm d}F(E_\nu)}{{\rm d}E_\nu} = c \int N_{\rm AGN}(z) n_{\rm ns/AGN} \frac{\overline{L}_\nu}{\langle E_\nu\rangle} \phi_\infty(E_\nu')(1+z) \left|\frac{{\rm d}t}{{\rm d}z}\right| {\rm d}z, \quad (25)$$

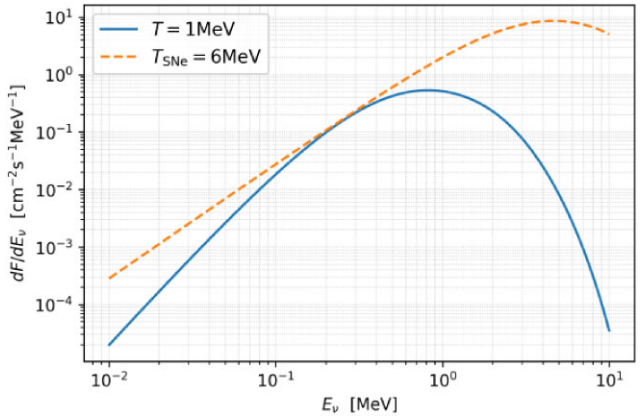

Figure 8. The neutrino background of all flavours produced by NS accretion in AGN discs (blue solid line). For comparison, the diffuse supernova neutrino background (yellow dashed line) of all flavours according to Horiuchi et al. (2009) is also presented.

where $E_\nu^{'} = E_\nu(1+z)$, $|\frac{\mathrm{d}z}{\mathrm{d}t}| = H_0(1+z)\left[\Omega_\mathrm{m}(1+z)^3+\Omega_\Lambda\right]^{1/2}$, and $\overline{L}_\nu$ is the average neutrino luminosity taking into account the duty cycle, as discussed in Section 4.2. In above equation, $N_\mathrm{AGN}(z)$ is the number density of AGN as a function of the cosmological redshift z, taken as:

$$N_\mathrm{AGN}(z) = N_\mathrm{AGN}(0)e(z), \tag{26}$$

where $N_\mathrm{AGN}(0) \sim 10^{-4}\mathrm{Mpc}^{-3}$ is the local AGN number density, and

$$e(z) = \begin{cases} (1+z)^{p_1}, & z \le z_\mathrm{c} \\ (1+z_\mathrm{c})^{p_1}\left(\frac{1+z}{1+z_\mathrm{c}}\right)^{p_2}, & z \ge z_\mathrm{c}, \end{cases} \tag{27}$$

with $p_1 = 4.1$, $p_2 = 0.03$, and $z_\mathrm{c} = 1.03$ (Ueda et al. 2003; Fotopoulou 2012). Within an AGN activity cycle of ~ 10 Myr, there have been $\sim 10^4$ NSs present (Perna et al. 2021). Consequently, the estimated average number of coexisting NS in an AGN disc is

$$n_\mathrm{ns/AGN} \sim \frac{10^4}{10\,\mathrm{Myr}}\frac{\eta \mathrm{M}_\odot c^2}{\overline{L}_\nu}. \tag{28}$$

Numerically, the integral above is computed up to the redshift of $z = 5$.

The blue curve in Fig. 8 shows the contribution of neutrinos produced by NSs accretion in AGN discs to the background. The neutrino background generated by NS accretion in AGN discs is primarily in the $\sim$ MeV energy range, while MeV neutrino background is mostly attributed to supernova contributions. The dotted orange line provides the diffuse supernova neutrino background for comparison (Horiuchi et al. 2009). Since the average energy of neutrinos produced by NS accretion is slightly lower than that from supernova, and supernova neutrinos are approximately thermal (Fermi-Dirac distribution), whereas the spectra of neutrinos produced by NS accretion is given by equation (21), therefore these two backgrounds are distinct. At the MeV range, the neutrino background produced by NS accretion in AGNs accounts for ~ 25 percent of the supernova neutrino background. Around 0.3 MeV, the neutrino background from NS accretion in AGNs is even comparable to that of supernova neutrinos.

It is noted that for neutrino backgrounds $\lesssim 1$MeV, they are primarily sourced from nuclear reactors on Earth, vastly surpassing the calculated neutrino background from NS accretion in AGN discs. However, reactor neutrinos originate from terrestrial sources and their locations are known, so the use of multiple detectors, as well as methods such as energy spectrum analysis and time correlation, may help differentiate between different signal sources and thus mitigate the impact of reactor neutrino. It is also worth noting that the number of NSs in the nuclear region has a significant impact on the background contribution. Mass segregation may reduce the number of NSs in the nuclear cluster of AGNs (McKernan et al. 2020), but repeated AGNs (Shankar, Weinberg & Miralda-Escudé 2009) would increase the number of NSs in the nuclear cluster, thereby increasing the contribution to the neutrino background.

3.4 Angular momentum carried away by neutrinos

Assuming that the generated neutrinos are emitted isotropically in the co-rotating frame of a NS with arguer velocity Ω, the rotation of the NS causes the neutrinos to potentially carry away angular momentum when observed from the laboratory frame. For ease of estimation, it is assumed that the rotation axis of the NS coincides with its magnetic pole and is perpendicular to the plane of the AGN disc. When the accretion flow travels along the accretion column towards the surface of the NS, it excites neutrinos. Each individual neutrino possesses momentum and, consequently, angular momentum. Evidently, in the co-rotating frame with the NS, the average angular momentum of neutrinos is zero. However, in the laboratory frame, the average angular momentum carried away by each neutrino with energy E_ν is:

$$\mathrm{d}\overline{J} = \frac{E_\nu \Omega \frac{r_\mathrm{cap}^2}{c^2}}{\sqrt{1-\frac{\Omega^2 r_\mathrm{cap}^2}{c^2}}}, \tag{29}$$

where the relationship between polar cap radius r_cap and magnetosphere radius r_m is (Shapiro & Teukolsky 2008)

$$r_\mathrm{cap} = r_\mathrm{ns}\sqrt{\frac{r_\mathrm{ns}}{r_\mathrm{m}}}. \tag{30}$$

Thus the total angular momentum loss rate due to neutrino emission is:

$$\dot{J} = \frac{\mathrm{d}N_\nu}{\mathrm{d}t}\mathrm{d}\overline{J} = \frac{L_\nu \Omega \frac{r_\mathrm{cap}^2}{c^2}}{\sqrt{1-\frac{\Omega^2 r_\mathrm{cap}^2}{c^2}}}. \tag{31}$$

Table 2 presents the angular momentum carried away by neutrinos, the angular momentum carried by the accretion flow, and their ratio for various NS masses and their rotational angular velocities. The ratio of angular momentum carried away by neutrinos is contingent on the location of neutrino emission as well as the position of the magnetosphere. The magnetosphere radius is maintained at 10^7cm in the table, but note that the ratio decreases slightly as the magnetosphere radius increases. According to the above estimates, there is evidence that while neutrinos can carry away the majority of the energy released from accretion, the angular momentum carried by neutrinos generally constitutes only a small fraction compared to the angular momentum of the accreting material. This is because neutrinos can only be emitted at the base of the accretion column. The remaining angular momentum will be transferred to the NS, contributing to its rotational acceleration or being balanced out by other mechanisms such as GWs.

4 GRAVITATIONAL WAVES IMPLICATIONS

NS accretion may have an impact on the GWs emitted by individual NSs, as well as on the GWs associated with the merger of binaries involving NSs.

Table 2. The rate of angular momentum loss carried away by neutrinos for various NS masses and their rotational angular velocities. From left to right, the columns represent: NS masses, rotational angular velocities of the NS, rates of angular momentum loss due to neutrino emissions, rates of angular momentum increase due to accretion, and the ratio of the above two quantities.

$m_{\rm ns}$ [$M_\odot$]	Ω (s^{-1})	$\dot{J}_\nu$ ($\frac{\dot{m}}{\dot{m}_{\rm Edd}}$ g cm^{2}s^{-2})	$\dot{J}_{\rm acc}$ ($\frac{\dot{m}}{\dot{m}_{\rm Edd}}$ g cm^{2}s^{-2})	$-\dot{J}_\nu/\dot{J}_{\rm acc}$
1.4	0	0	4.22×10^{34}	0
1.4	3.0×10^3	-1.12×10^{32}	4.22×10^{34}	0.27 per cent
1.4	$\Omega_{\rm K}$	-3.48×10^{32}	4.22×10^{34}	0.82 per cent
2.2	$\Omega_{\rm K}$	-7.18×10^{33}	5.29×10^{34}	1.36 per cent

4.1 GWs from NS mountains

The mass quadrupole of a NS is referred to as the 'mountains' of the NS, primarily arising from non-axisymmetric deformations in the crust. Accretion asymmetries onto the NS can lead to asymmetries in composition and heating, which in turn result in deformations of the NS and the generation of a quadrupole moment. These compositional and heating asymmetries may originate from the gravitational potential energy released by accretion itself, or from nuclear reactions within the NS. An accreting NS in AGN discs undergoes a series of nuclear reactions on its surface and crust, such as electron capture, neutron emission, and pycnonuclear reactions (Meisel et al. 2018). These nuclear reactions give rise to the quadrupolar component of temperature variation, contributing to the asymmetric heating of the crust and consequently raising the mass quadrupole. Furthermore, Ushomirsky et al. (2000) illustrates the trend of increasing mass quadrupole with an increasing accretion rate.

While there remains uncertainty regarding the heating asymmetry induced by nuclear reactions, continuous accretion of the NS allows for mountains to be built incrementally, eventually reaching the maximum quadrupole (Ushomirsky et al. 2000). This maximum quadrupole exists because large stresses can break the crust (Horowitz & Kadau 2009). Haskell et al. (2015) provide the maximum quadrupole that can be sustained in the NS crust, up to $Q_{22}\sim10^{40}$g cm^2. This maximum quadrupole consequently places an upper limit on the GW strain. The relationship between the mass quadrupole and strain is described by (Ushomirsky et al. 2000)

$$h_{\rm a1}=\frac{16}{5}\left(\frac{\pi}{3}\right)^{\frac{1}{2}}\frac{GQ_{22}\Omega^2}{dc^2}, \tag{32}$$

where d is the distance to the source.

In many studies, it is assumed that GWs can balance out the angular momentum brought about by accretion (Papaloizou & Pringle 1978; Wagoner 1984; Bildsten 1998). However, due to the high accretion rate of NSs in AGN discs, which can exceed $\gtrsim10^5\dot{m}_{\rm Edd}$ as discussed in Section 2.3, even if the mass quadrupole of the NS crust reaches its maximum limit, the emitted GWs may not be sufficient to balance the angular momentum from accretion. Nevertheless, if the mass quadrupole induced by the magnetic field is considered, it may not be constrained by the aforementioned limit on crustal deformation. This could lead to the generation of a larger mass quadrupole, potentially balancing out the angular momentum from accretion. In this scenario, the corresponding strain would be

$$h_{\rm a2}=\left(\frac{G\dot{m}}{\Omega c^3}\right)^{\frac{1}{2}}\frac{(Gm_{\rm ns}r_{\rm m})^{\frac{1}{4}}}{d}. \tag{33}$$

Fig. 9 illustrates the sensitivity of GW detectors and the potential upper limits of GWs generated by NS accretion. An integration

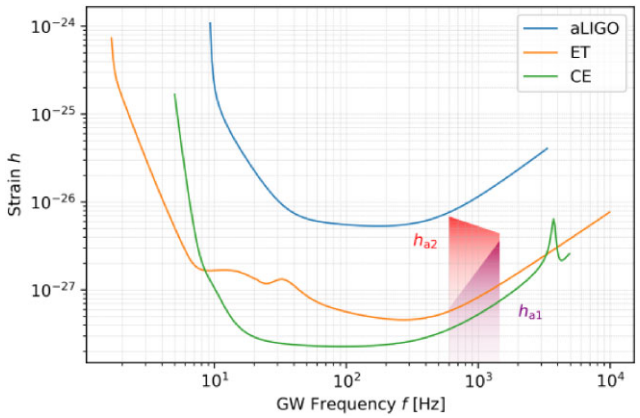

Figure 9. The GW strain range produced by the accretion of a NS in a nearby AGN disc. The purple region represents the potential strain corresponding to the maximum quadrupole moment that the crust can sustain, while the red region represents the range of strain when the angular momentum lost from GWs balances with the accretion flow. The rotation frequencies of the NS is chosen within the range of 300–730 Hz, resulting in GW frequencies within the range of 600–1460 Hz. For comparison, various sensitivity curves of detectors are shown.

search over a time period, $t_{\rm obs}$, is capable of detecting a strain of

$$h\approx11.4\sqrt{\frac{S_{\rm n}(f)}{t_{\rm obs}}}, \tag{34}$$

where $S_{\rm n}(f)$ is the detector's noise power spectral density, and the factor 11.4 accounts for a false dismissal rate of 10 per cent and a false alarm rate of 1 per cent per single trial (Abbott et al. 2007). The strain sensitivity curves (i.e. $S_{\rm n}(f)$) for Advanced LIGO (aLIGO), Einstein Telescope (ET), and Cosmic Explorer (CE) are derived from Moore, Cole & Berry (2015). For the detectors depicted in the graph, an observation time of $t_{\rm obs}=2$yr has been chosen. Regarding the GWs produced by NS accretion in AGN discs, a source distance of $d=5$Mpc is assumed, which exceeds the nearest known AGN (Filippenko & Ho 2003). Two potential upper limits of GWs are considered: the purple region in the graph represents the possible strain corresponding to the maximum quadrupole that the crust can sustain, while the red region represents the range of strain when the accretion rate is $\sim2\times10^5\dot{m}_{\rm Edd}$, balancing the angular momentum from accretion. Both of these potential upper limits lie above the sensitivity curves for ET and CE. Therefore, GWs generated by NS accretion in AGN discs may potentially be detected by third-generation GW detectors within 2 yr.

The GWs may also exhibit several characteristic effects due to the environment within the AGN disc, especially the presence of the SMBH. These effects include: (i) Periodic modulations in the GW signal due to changing path length along the line of sight during

the NS's orbit around the SMBH. (ii) Relativistic beaming, Doppler, and gravitational redshift leading to a phase shift in the GW signal. (iii) The variation of 'light' traveltime in the gravitational field of the SMBH, known as the Shapiro delay (Meiron, Kocsis & Loeb 2017). (iv) Gravitational lensing effect causing the production of GW echoes (Gondán & Kocsis 2022). The GW echo exhibits a time-frequency evolution very similar to the primary signal but arrives after a time delay. Moreover, the NSs in AGN discs undergo intermittent accretion, leading to potentially intermittent GW emissions, as illustrated in the next subsection. Combined with these effects, GW signals from NSs in AGN discs and those in X-ray binaries (Bildsten 1998; Watts et al. 2008) could be differentiated. If the GWs produced by the accretion of NSs in AGN discs are detected, the presence of NS in AGN discs can be confirmed, consequently revealing the astrophysics of compact objects in AGN discs.

The extraction of angular momentum by GWs from a NS is crucial. For instance, Pan & Yang (2021b), when considering whether accretion onto a NS can lead to the shedding limit, found that the results were marginal. They observed that for different parameters, the outcomes varied, but in most cases, the results were situated at the boundary between being able to reach the shedding limit and not. However, their calculations did not account for angular momentum loss. Therefore, even if GWs can carry away some angular momentum during the accretion process, it becomes less likely for NSs in AGN discs to reach the shedding limit. This allows accretion to continue, making collapse more likely to occur.

4.2 Implications for binary NS merger

In AGN discs, the accretion of NSs involves feedback to the AGN gas. This alters the accretion rate, consequently affecting the merger rate. If the NS continues to accrete at a hyper-Eddington rate, it will quickly exceed its critical mass and collapse, making binary NS mergers less likely to occur in AGN discs. However, the circum-NS disc is dominated by outflows, which provide feedback into the AGN disc, creating a cavity, and then subsequently returning to the hyper-Eddington rate again. Therefore, the duty cycle induced by this feedback needs to be considered.

Feedback calculations follow Chen et al. (2023), but we also take into account that neutrinos in the NS process carry away most of the released gravitational potential energy. Therefore, the only feedback effect come from the wind of circum-NS disc. The time-scale for the circum-NS disc to maintain effective accretion is

$$t_{\rm acc} = \alpha^{-1} h^{-2} \Omega_{\rm K}^{-1}, \tag{35}$$

where $\alpha \sim \tilde{\alpha}$, $h \sim 0.5$, and $\Omega_{\rm K}$ are the viscosity, the height ratio, and the Keplerian angular velocity of the circum-NS disc respectively. The wind from the circum-NS disc interacts with the surrounding AGN disc gas through a forward shock, creating a shell of shocked disc gas separated by the shocked outflow material. The radius of the expanding shell change over time as (Weaver et al. 1977)

$$r_{\rm shell} = 0.88 \left(\frac{L_{\rm w} t^3}{\tilde{\rho}_0} \right)^{\frac{1}{5}}, \tag{36}$$

where $L_{\rm w}(\dot{m}_{\rm rel}, r_{\rm cir}, r_{\rm m}, s)$ is the heat inject rate into the AGN disc through the wind of the circum-NS disc (Chen et al. 2023). The breakout time-scale, $t_{\rm bre}$, can be calculated from $r_{\rm shell}(t_{\rm bre}) = \tilde{H}$. The formation and recovery times of the cavity are related to the two times, $t_{\rm acc}$ and $t_{\rm bre}$. The time for the expansion of the cavity outwards is

$$t_{\rm cav} = \begin{cases} \frac{r_{\rm cav}^3 - r_{\rm shellb}^3(t_{\rm acc})}{3 r_{\rm shellb}^2(t_{\rm acc}) v_{\rm shellb}(t_{\rm acc})} + t_{\rm acc}, & t_{\rm acc} \gtrsim t_{\rm bre} \\ \frac{r_{\rm cav}^3 - \tilde{H}^3}{3 \tilde{H}^2 v_{\rm shellE}(t_{\rm breE})} + t_{\rm breE}, & t_{\rm acc} \lesssim t_{\rm bre}, \end{cases} \tag{37}$$

where

$$r_{\rm cav} = \begin{cases} \left[r_{\rm shellb}^2(t_{\rm acc}) v_{\rm shellb}(t_{\rm acc}) / \tilde{c}_{\rm s} \right]^{\frac{1}{2}}, & t_{\rm acc} \gtrsim t_{\rm bre} \\ \left[r_{\rm shellE}^2(t_{\rm breE}) v_{\rm shellE}(t_{\rm breE}) / \tilde{c}_{\rm s} \right]^{\frac{1}{2}}, & t_{\rm acc} \lesssim t_{\rm bre}. \end{cases} \tag{38}$$

In the case of $t_{\rm acc} \gtrsim t_{\rm bre}$, $r_{\rm shellb}(t)$ and $v_{\rm shellb}(t)$ are the radius and velocity of the expanding shell after the shock break out, and in the case of $t_{\rm acc} \lesssim t_{\rm bre}$, $r_{\rm shellE}(t_{\rm breE})$ and $v_{\rm shellE}(t_{\rm breE})$ are the radius and velocity of the expanding shell at the moment of the shock break out, following Chen et al. (2023). The recovery time-scale of the cavity can be estimated as the radius over the local sound speed, i.e.

$$t_{\rm ref} = \frac{r_{\rm cav}}{\tilde{c}_{\rm s}}. \tag{39}$$

Therefore, the duty cycle is defined as

$$\xi = \frac{t_{\rm acc}}{t_{\rm cav} + t_{\rm ref}}. \tag{40}$$

After considering the feedback, the average accretion rate of NSs needs to be multiplied by this duty cycle based on Section 2.3. The collapse time-scale consequently is

$$\tau_{\rm coll} \sim \frac{\rm M_\odot}{\xi \dot{m}}. \tag{41}$$

Fig. 10 shows the duty cycle of NS accretion and the time-scale of accretion-induced collapse in the fiducial model. In comparison to the scenario with BH (Chen et al. 2023), the relatively large duty cycle of NS accretion is attributed to the influence of magnetic fields and neutrino production. Furthermore, Chen et al. (2023) also takes into account the feedback from accretion of NSs onto AGN discs, but does not consider neutrinos generated by NS accretion. Instead, it assumes that the released gravitational energy is entirely utilized for feedback on the gas in the AGN disc. Consequently, their work overestimates the feedback from NS accretion, resulting in a smaller duty cycle. Actually, the larger duty cycle make it more likely for NSs in the AGN disc to collapse due to accretion. This is justified by the comparison of the migration time-scale. We take into consideration Type I migration as well as migration due to GW released. While there are additional factors influencing migration, they are not expected to significantly alter the order of magnitude of the migration time-scale. In the right panel of Fig. 10, the yellow curve represents the migration time-scale of NSs in the AGN disc. It can be observed that in the fiducial model, the migration time-scale is greater than the collapse time-scale, which is also shorter than the typical lifetime of an AGN ($\sim$ 10Myr). In AGN discs, binary objects typically form in regions with differential migration or migration traps. Consequently, the migration time-scale can serve as a lower limit for the time-scale of binary mergers. Clearly, binary NS mergers are unlikely to occur in AGN discs.

Not limited to the fiducial model, Fig. 11 provides comparisons between the collapse time-scale and the migration time-scale in various cases, and the results generally agree with those of the fiducial model, i.e. the accretion time-scale is shorter than the migration time-scale. This implies that NSs in AGN discs may collapse before anticipated collisions or mergers. The only exception arises from smaller mass SMBHs in AGNs, where the collapse time-scale may exceed the migration time-scale, as shown in the upper left panel of Fig. 11. Luo et al. (2023) simulated hierarchical triple systems

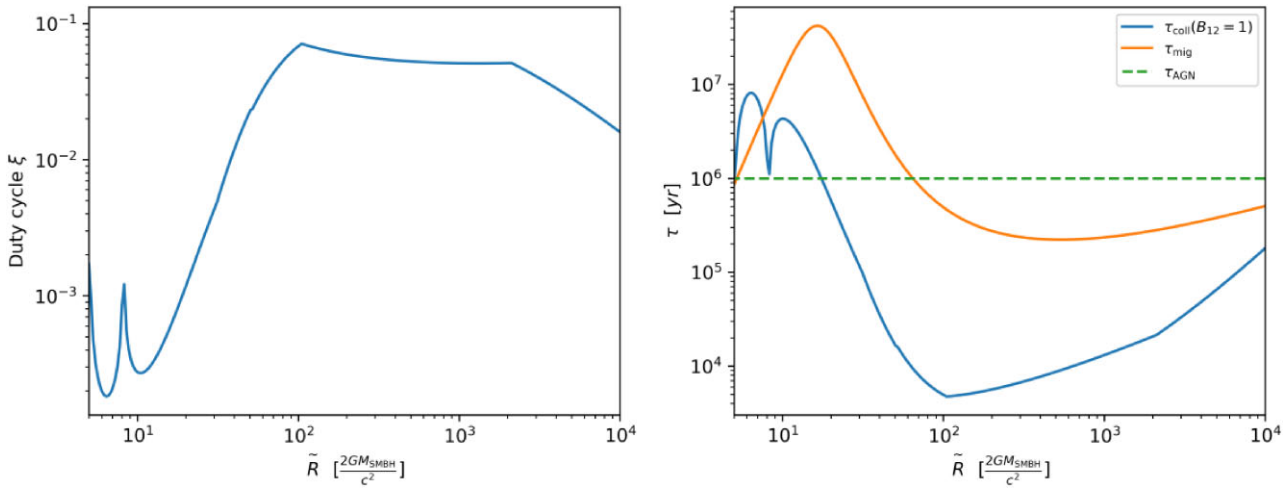

Figure 10. Left panel: Duty cycle of NS accretion in the AGN disc at different disc radii in the fiducial model. Right panel: Time-scales of NS accretion collapse (blue) and migration (yellow) in the AGN disc with fiducial parameters.

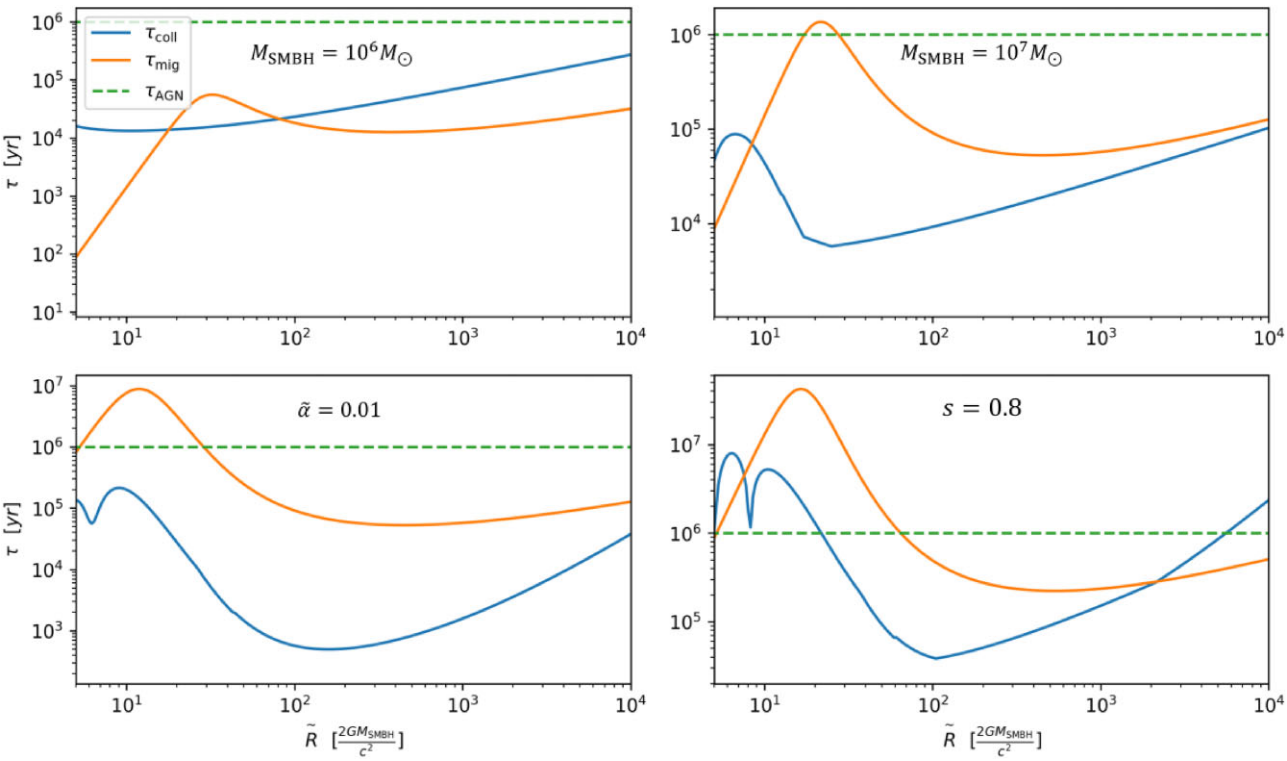

Figure 11. Time-scales of NS accretion collapse (blue) and migration (yellow) in AGN discs with parameters beyond the fiducial values. The upper left panel is for $M_{\rm SMBH} = 10^6 {\rm M}_\odot$, the upper right panel is for $M_{\rm SMBH} = 10^7 {\rm M}_\odot$, the lower left panel is for $\tilde{\alpha} = 0.01$, and the lower right panel is for $s = 0.8$ in equation (10). The remaining parameters are consistent with those of the fiducial model.

composed of a binary star and the SMBH in AGN discs, and the results indicate that smaller SMBHs are more likely to lead to binary mergers or collisions. However, it is important to note that this likelihood is relative. When compared to WDs in AGN discs, NS mergers are still rare, as they require the emission of GWs to bring the two NSs within the capture radius. Indeed, our findings are consistent with observations. As of 2024 May 15, ground-based GW observatories have detected nearly 200 GW sources. However, among them, only two binary NS merger events have been confirmed (GW170817 and GW190425), along with about five potential NS-BH merger events (LIGO 2024).

It is worth noting that when matter falls onto the surface of a NS, the majority of the released energy is carried away by neutrinos, but due to the high opacity of AGN discs, a small fraction of energy in the form of electromagnetic radiation ($\sim L_{\rm Edd}$) is still injected into the AGN disc. However, compared to the outflow from the circum-NS disc to the AGN discs, it is negligible. Additionally, for NSs in AGN discs, the dipole magnetic field truncates the circum-NS disc

at larger radii, reducing its outflow. Therefore, compared to BHs in AGN discs, the feedback from NSs is smaller.

5 DISCUSSION

Apart from neutrinos and GWs effects, accretion of NSs in AGN discs may still have electromagnetic effects.[2] Due to the dominance of outflows in the circum-NS disc, the cavities formed by its feedback onto the AGN disc may potentially cause shocks to break out on the surface of the AGN disc and propagate into the broad-line region. The momentum-driven outflow may even fall back under the gravity of the central SMBH. These processes subsequently could result in radiation across various bands including radio, optical, UV, soft X-ray, and even GeV (Wang et al. 2021; Chen et al. 2023). While the direct observational effects may be relatively weak, this could lead to the AGN disc becoming feedback-dominant (Gilbaum & Stone 2022). Additionally, magnetic reconnection following the collapse of the accreted NS may trigger phenomena similar to fast radio bursts (FRBs) (Falcke & Rezzolla 2014; Perna et al. 2021).

Because the circum-NS disc has a significant impact on the rotational angular velocity of the NS as well as the accretion feedback onto the AGN disc, here are some necessary caveats to note. Currently, it is assumed that the NS accretes material from the Keplerian AGN disc, although turbulence may be present on the AGN disc. Turbulence could potentially lead to the disappearance of the circum-NS disc (Chen & Lin 2023). In this scenario, the accretion pattern of the NS resembles the spherical accretion depicted in Fig. 5. Furthermore, when the NS orbit exhibits eccentricity around the SMBH, it results in retrograde accretion, potentially causing the circum-NS disc to even reverse its direction (Chen et al. 2022; Li et al. 2022a).

A uniform density within the scale height of the AGN disc is assumed in this study. However, this assumption does not adequately account for the disc's geometry and the impact of pressure gradient forces resulting from free expansion perpendicular to the AGN disc plane. When considering the disc's vertical structure, the evolution of the cavity's shape, scale, and breakout position may be altered (Mac Low & McCray 1988; Tagawa et al. 2022). Moreover, the evolution of the cavity is not solely governed by momentum conservation; thermal pressure may also contribute to the displacement of the shell. Considering these factors, our estimates may require adjustments, although our results remain reasonable in magnitude and do not alter the fundamental physical picture.

Magnetic fields play a crucial role in neutrino production, feedback onto the AGN disc, and the evolution of NS. While massive stars evolving in AGN discs may possess a higher proportion of magnetars ($\gtrsim 10^{13}$G), their subsequent evolution is complex. The magnetic field may decrease during accretion due to processes like Ohmic dissipation, stabilizing at an estimated $\sim 10^{9} - 10^{10}$G (Pan & Yang 2021b). On the other hand, magnetic fields are commonly assumed in disc models (Eardley & Lightman 1975), and average values of $\sim 10^{4}$ G are observed in AGN discs (Silant'ev et al. 2009; Daly 2019). When the NS accretes material from the AGN disc, the NS's magnetic field may be amplified due to magnetic flux conservation during the accretion process. Performing magnetohydrodynamic numerical simulations of these processes in future work would be of great interest. Additionally, the dipole magnetic field is assumed in this study. In reality, both theoretical and observational evidence suggest the existence of multipole fields (e.g. Roberts 1979; Gil & Mitra 2001; Pétri 2015). If they are prevalent, accretion columns may not form. Due to the significant uncertainty introduced by the configuration of multipole fields, their effects are not accounted for in this study.

Strong magnetic fields and rapidly rotating NSs (e.g. $B \gtrsim 10^{13}$ G and $f \gtrsim 100$ Hz) may also induce the propeller effect during the accretion process, resulting in a reduction in the accretion rate (e.g. Davidson & Ostriker 1973; Parfrey, Spitkovsky & Beloborodov 2016). However, for NSs with weaker magnetic fields, the magnetospheric radius $r_{\rm m}$ may be smaller than or comparable to the corotation radius, in which case the propeller effect does not occur. Furthermore, even if $r_{\rm m}$ is slightly larger than the corotation radius, accretion onto the NS is not abruptly hindered in the mild propeller regime (Ghosh & Lamb 1979; Pan & Yang 2021b). It is also worth noting that our model inherently supports intermittent accretion onto NSs in AGN discs, thus encompassing the occurrence of the propeller effect. In cases where the propeller effect occurs, the still high accretion rate at the Bondi radius and the sharply reduced accretion rate onto the NS surface inevitably lead to an increase in the wind, enhancing the feedback on the AGN disc. This corresponds to the parameter 's' in equation (10) increase. Due to the complexity of the physical processes involved, we currently only assume 's' to be a free parameter.

The investigation of nucleosynthesis in accreted matter and their impact on the NS's mass quadrupole moment warrants further exploration. Extensive research has been conducted on nuclear reactions within the surface and crust of NSs. However, accretion onto NSs in AGN discs is highly intense and may involve strong magnetic fields. The nature of nuclear reactions in such an environment remains unclear. It is currently understood in a qualitative sense that high accretion rates may lead to continuous, rather than intermittent, nuclear reactions on the surface (Meisel et al. 2018). The strong magnetic field can change the structure of the outer layer of NSs (Chamel & Haensel 2008; Meisel et al. 2018), thereby influencing nucleosynthesis. The composition and asymmetry in heating of the NS's crust heavily rely on these nuclear reactions, consequently influencing GWs.

Currently, we are conducting qualitative studies of various characteristic models or stages, without delving into the continuously dynamical evolution. For instance, the physics at the junction of different-scale accretion models, and the evolution over time of accretion columns and the circum-NS disc, remain unclear. The spin and magnetic field of NSs can further influence the critical mass for NS collapse, although this is not expected to significantly impact our qualitative estimates. These aspects warrant future investigation through precise numerical simulations to elucidate their intricate structures and evolution.

6 CONCLUSIONS

In this work, we study the accretion of NSs in AGN discs at various scales. Through the analysis of characteristic effects in both AGN discs and NSs, the accretion rate of NSs and its feedback are determined, as well as multimessenger implications are illustrated, leading to the following concluding remarks.

(i) Accretion of NSs in AGN discs exhibits a hierarchical structure (Fig. 1). It occurs in an approximately spherical manner on Bondi scales. On scales near the NS by one to two orders of magnitude, a circum-NS disc forms due to the differential rotation of AGN disc gas. As the accretion flow approaches the magnetosphere of the NS, the magnetic field guides the accretion flow, forming accretion columns that flow towards the NS with hyper-Eddington rates (Figs 2 and 4).

[2]Additional details are available in the supplementary material.

More generally, various possible states of NS accretion in AGN discs are classified in Fig. 5.

(ii) The hard surface of a NS leads to a high energy efficiency of accretion. Possible strong magnetic fields can channel accretion material towards narrow accretion columns. Thus, the hyper-Eddington accreting NSs in AGN discs can generate neutrinos through positron–electron annihilation. Neutrinos carry away excess energy, imposing an upper limit on electromagnetic radiation. The neutrino energy spectrum is the non-thermal spectrum corresponding to neutrinos that can freely escape (Fig. 7), with a characteristic temperature of approximately 1 MeV at the position of neutrino production (Table 1). Neutrinos produced by NS accretion make a significant contribution to the sub-MeV and MeV background, even comparable to the contribution from supernovae at around 0.3 MeV (Fig. 8).

(iii) Accretion onto a NS can also lead to the generation of mass quadrupole, resulting in the emission of GWs. The corresponding upper limit on strain may be detectable by third-generation GW detectors (Fig. 9), and these GWs can exhibit characteristic effects such as Doppler shifts and echoes. GWs could extract angular momentum from the accretion flow (Table 2), alleviating the shedding limit and enabling sustained accretion.

(iv) The magnetosphere potentially truncates the circum-NS disc at a larger radius $r_{\rm m}$, which in turn reduces the outflow from the circum-NS disc, thereby diminishing the feedback on AGNs. Generally, the duty cycle is relatively large, with the average accretion-collapse time-scale being shorter than the migration (and therefore merger) time-scales in AGN discs (Figs 10 and 11). As a result, NS accretion-collapses tend to manifest in AGN discs before the occurrence of binary mergers.

To sum up, the accretion of NSs in AGN discs is crucial. Combining further numerical simulation and multimessenger observations holds promise in confirming the presence of compact objects in AGN disc, providing insights into the physics of their extreme environments, and identifying potential hosts of GW sources.

ACKNOWLEDGEMENTS

We thank the referee for critical suggestions and comments, which are very helpful for the improvement of this work. The authors would like to thank Alexander A. Mushtukov for his explanations of the pair production process in his paper. SRZ acknowledges support from China Scholarship Council (CSC No. 202206340085). YFY is supported by National Natural Science Foundation of China (Grant No. 12393812), National SKA Program of China (Grant No. 2020SKA0120300) and the Strategic Priority Research Program of the Chinese Academy of Sciences (Grant No. XDB0550200). JMW acknowledges support from the National Key R&D Program of China (2020YFC2201400, 2021YFA1600404), NSFC (NSFC-11991050, -11991054, -11833008). LCH was supported by the National Science Foundation of China (11991052, 12233001), the National Key R&D Program of China (2022YFF0503401), and the China Manned Space Project (CMS-CSST-2021-A04, CMS-CSST-2021-A06).

DATA AVAILABILITY

The data underlying this article will be shared on reasonable request to the corresponding author (YFY).

REFERENCES

Abbott B. et al., 2007, Phys. Rev. D, 76, 082001
Abbott B. P. et al., 2017, Phys. Rev. Lett., 119, 161101
Abbott B. P. et al., 2020a, ApJ, 892, L3
Abbott R. et al., 2020b, ApJ, 896, L44
Abbott R. et al., 2021, ApJ, 915, L5
Abe K. et al., 2011, preprint (arXiv:1109.3262)
Andersson N., 1998, ApJ, 502, 708
Andersson N., Kokkotas K. D., Stergioulas N., 1999, ApJ, 516, 307
Asthana A., Mushtukov A. A., Dobrynina A. A., Ognev I. S., 2023, MNRAS, 522, 3405
Bahcall J. N., 1989, Neutrino Astrophysics. Cambridge Univ. Press, Cambridge
Bartos I., Kocsis B., Haiman Z., Márka S., 2017, ApJ, 835, 165
Basko M. M., Sunyaev R. A., 1976, MNRAS, 175, 395
Beacom J. F., 2010, Annu. Rev. Nucl. Part. Sci., 60, 439
Bellovary J. M., Mac Low M.-M., McKernan B., Ford K. E. S., 2016, ApJ, 819, L17
Bernal C. G., Lee W. H., Page D., 2010, Rev. Mex. Astron. Astrofis., 46, 309
Bildsten L., 1998, ApJ, 501, L89
Bildsten L., Brown E. F., 1997, ApJ, 477, 897
Blandford R. D., Begelman M. C., 1999, MNRAS, 303, L1
Cantiello M., Jermyn A. S., Lin D. N. C., 2021, ApJ, 910, 94
Chamel N., Haensel P., 2008, Living Rev. Relat., 11, 10
Chen Y.-X., Lin D. N. C., 2023, MNRAS, 522, 319
Chen Y.-X., Bailey A., Stone J., Zhu Z., 2022, ApJ, 939, L23
Chen K., Ren J., Dai Z.-G., 2023, ApJ, 948, 136
Cheng K. S., Wang J.-M., 1999, ApJ, 521, 502
Chevalier R. A., 1989, ApJ, 346, 847
Chevalier R. A., 1995, Phys. Rep., 256, 95
Chevalier R. A., 1996, ApJ, 459, 322
Daly R. A., 2019, ApJ, 886, 37
Davidson K., Ostriker J. P., 1973, ApJ, 179, 585
Derdzinski A., Mayer L., 2023, MNRAS, 521, 4522
Dittmann A. J., Miller M. C., 2020, MNRAS, 493, 3732
Dittmann A. J., Cantiello M., Jermyn A. S., 2021, ApJ, 916, 48
Eardley D. M., Lightman A. P., 1975, ApJ, 200, 187
Fabj G., Nasim S. S., Caban F., Ford K. E. S., McKernan B., Bellovary J. M., 2020, MNRAS, 499, 2608
Falcke H., Rezzolla L., 2014, A&A, 562, A137
Filippenko A. V., Ho L. C., 2003, ApJ, 588, L13
Ford K. E. S., McKernan B., 2022, MNRAS, 517, 5827
Fotopoulou S., 2012, PhD thesis, Technische Universitaet Muenchen, Germany
Ghosh P., Lamb F. K., 1979, ApJ, 234, 296
Gil J., Mitra D., 2001, ApJ, 550, 383
Gilbaum S., Stone N. C., 2022, ApJ, 928, 191
Gondán L., Kocsis B., 2022, MNRAS, 515, 3299
Harding A. K., Lai D., 2006, Rep. Prog. Phys., 69, 2631
Haskell B., Priymak M., Patruno A., Oppenoorth M., Melatos A., Lasky P. D., 2015, MNRAS, 450, 2393
Horiuchi S., Beacom J. F., Dwek E., 2009, Phys. Rev. D, 79, 083013
Horowitz C. J., Kadau K., 2009, Phys. Rev. Lett., 102, 191102
Houck J. C., Chevalier R. A., 1991, ApJ, 376, 234
Jermyn A. S., Dittmann A. J., Cantiello M., Perna R., 2021, ApJ, 914, 105
Kaminker A. D., Gnedin O. Y., Yakovlev D. G., Amsterdamski P., Haensel P., 1992, Phys. Rev. D, 46, 4133
Kaminker A. D., Gnedin O. Y., Yakovlev D. G., Amsterdamski P., Haensel P., 1994, Astron. Astrophys. Trans., 4, 283
Kathirgamaraju A., Li H., Ryan B. R., Tchekhovskoy A., 2023, preprint (arXiv:2311.03571)
Kato S., Fukue J., Mineshige S., 2008, Black-Hole Accretion Disks. Kyoto University Press, Kyoto Japan
Konar S., Bhattacharya D., 1997, MNRAS, 284, 311
Kotake K., Sato K., Takahashi K., 2006, Rep. Prog. Phys., 69, 971
GraceDB, 2024, GraceDB | The Gravitational-Wave Candidate Event Database. Available at: https://gracedb.ligo.org/
Li Y.-P., Chen Y.-X., Lin D. N. C., Wang Z., 2022a, ApJ, 928, L1
Li J., Lai D., Rodet L., 2022b, ApJ, 934, 154
Luo Y., Wu X.-J., Zhang S.-R., Wang J.-M., Ho L. C., Yuan Y.-F., 2023, MNRAS, 524, 6015

Mac Low M.-M., McCray R., 1988, ApJ, 324, 776
McKernan B., Ford K. E. S., O'Shaughnessy R., 2020, MNRAS, 498, 4088
Meiron Y., Kocsis B., Loeb A., 2017, ApJ, 834, 200
Meisel Z., Deibel A., Keek L., Shternin P., Elfritz J., 2018, J. Phys. G Nucl. Phys., 45, 093001
Melatos A., Payne D. J. B., 2005, ApJ, 623, 1044
Misiaszek M., Odrzywołek A., Kutschera M., 2006, Phys. Rev. D, 74, 043006
Mohapatra R. N., Pal P. B., 2004, Massive Neutrinos in Physics and Astrophysics, 3rd Edn. World Scientific
Moore C. J., Cole R. H., Berry C. P. L., 2015, Class. Quantum Gravity, 32, 015014
Mushtukov A. A., Tsygankov S. S., Suleimanov V. F., Poutanen J., 2018, MNRAS, 476, 2867
Mushtukov A. A., Ognev I. S., Nagirner D. I., 2019, MNRAS, 485, L131
Netzer H., 2013, The Physics and Evolution of Active Galactic Nuclei. Cambridge Univ. Press, Cambridge
Ostriker J. P., 1983, ApJ, 273, 99
Özel F., Psaltis D., Narayan R., Santos Villarreal A., 2012, ApJ, 757, 55
PSNS, 2001, PSNS – Pre Supernova Neutrino Spectrum homepage. Available at: http://th.if.uj.edu.pl/ odrzywolek/psns/index.html
Pan Z., Yang H., 2021a, Phys. Rev. D, 103, 103018
Pan Z., Yang H., 2021b, ApJ, 923, 173
Pan Z., Lyu Z., Yang H., 2022, Phys. Rev. D, 105, 083005
Papaloizou J., Pringle J. E., 1978, MNRAS, 184, 501
Parfrey K., Spitkovsky A., Beloborodov A. M., 2016, ApJ, 822, 33
Perna R., Tagawa H., Haiman Z., Bartos I., 2021, ApJ, 915, 10
Pétri J., 2015, MNRAS, 450, 714
Planck Collaboration VI, 2020, A&A, 641, A6
Raynaud R., Guilet J., Janka H.-T., Gastine T., 2020, Sci. Adv., 6, eaay2732
Roberts W. J., 1979, ApJS, 41, 75
Ruffini R., Wilson J., 1973, Phys. Rev. Lett., 31, 1362
Samsing J. et al., 2022, Nature, 603, 237
Scholberg K., 2015, in Feldman G., ed., XXVI International Conference on Neutrino Physics and AstroPhysics: Neutrino 2014. AIPCP, US, p. 070002
Shakura N. I., Sunyaev R. A., 1973, A&A, 24, 337
Shankar F., Weinberg D. H., Miralda-Escudé J., 2009, ApJ, 690, 20
Shapiro S. L., Teukolsky S. A., 2008, Black Holes, White Dwarfs, and Neutron Stars: The Physics of Compact Objects. John Wiley and Sons, United States
Silant'ev N. A., Piotrovich M. Y., Gnedin Y. N., Natsvlishvili T. M., 2009, A&A, 507, 171
Sirko E., Goodman J., 2003, MNRAS, 341, 501
Stone N. C., Metzger B. D., Haiman Z., 2017, MNRAS, 464, 946
Syer D., Clarke C. J., Rees M. J., 1991, MNRAS, 250, 505
Tagawa H., Haiman Z., Kocsis B., 2020, ApJ, 898, 25
Tagawa H., Kocsis B., Haiman Z., Bartos I., Omukai K., Samsing J., 2021, ApJ, 908, 194
Tagawa H., Kimura S. S., Haiman Z., Perna R., Tanaka H., Bartos I., 2022, ApJ, 927, 41
Tanaka H., Takeuchi T., Ward W. R., 2002, ApJ, 565, 1257
Ueda Y., Akiyama M., Ohta K., Miyaji T., 2003, ApJ, 598, 886
Ushomirsky G., Cutler C., Bildsten L., 2000, MNRAS, 319, 902
Wagoner R. V., 1984, ApJ, 278, 345
Wang J.-M., Liu J.-R., Ho L. C., Du P., 2021, ApJ, 911, L14
Watts A. L., Krishnan B., Bildsten L., Schutz B. F., 2008, MNRAS, 389, 839
Weaver R., McCray R., Castor J., Shapiro P., Moore R., 1977, ApJ, 218, 377
Yang Y., Bartos I., Haiman Z., Kocsis B., Márka Z., Stone N. C., Márka S., 2019, ApJ, 876, 122
Yang Y., Gayathri V., Bartos I., Haiman Z., Safarzadeh M., Tagawa H., 2020, ApJ, 901, L34
Zel'dovich Y. B., Ivanova L. N., Nadezhin D. K., 1972, Sov. Astron., 16, 209
Zhang S.-R., Luo Y., Wu X.-J., Wang J.-M., Ho L. C., Yuan Y.-F., 2023, MNRAS, 524, 940
Zhu J.-P., Zhang B., Yu Y.-W., Gao H., 2021, ApJ, 906, L11

SUPPORTING INFORMATION

Supplementary data are available at *MNRAS* online.

suppl_data

Please note: Oxford University Press is not responsible for the content or functionality of any supporting materials supplied by the authors. Any queries (other than missing material) should be directed to the corresponding author for the article.

This paper has been typeset from a TEX/LATEX file prepared by the author.